sustainability

MDPI

Article

An Innovative LFC System Using a Fuzzy FOPID-Enhanced via PI Controller Tuned by the Catch Fish Optimization Algorithm Under Nonlinear Conditions

Saleh Almutairi [1,*], Fatih Anayi [1], Michael Packianather [1] and Mokhtar Shouran [2]

[1] School of Engineering, Cardiff University, Cardiff CF24 3AA, UK; anayi@cardiff.ac.uk (F.A.); packianatherms@cardiff.ac.uk (M.P.)
[2] Libyan Centre for Engineering Research and Information Technology, Bany Walid P.O. Box 38645, Libya; mokhta4520@gmail.com
* Correspondence: almutairis3@cardiff.ac.uk

Abstract

Load frequency control (LFC) remains a critical challenge in ensuring the stability of modern power grids. The integration of nonlinear dynamics into LFC design is paramount to achieving robust performance, which directly underpins grid reliability. This study introduces a novel hybrid control strategy—a fuzzy fractional-order proportional–integral–derivative (Fuzzy FOPID) controller augmented with a proportional–integral (PI) compensator—for LFC applications in two distinct dual-area interconnected power systems. To optimize the controller's parameters, the recently developed Catch Fish Optimization Algorithm (CFOA) is employed, leveraging the Integral Time Absolute Error (ITAE) as the primary cost function for precision tuning. A comprehensive comparative analysis is conducted to benchmark the proposed controller against the existing methodologies documented in the literature. Nonlinear elements' impact on the system stability is also investigated. The investigation evaluates the impact of critical nonlinearities, including governor dead band (GDB) and generation rate constraints (GRCs), on system performance. The simulation results demonstrate that the CFOA-tuned Fuzzy FOPID + PI controller exhibits superior robustness and dynamic response compared to conventional approaches, effectively mitigating frequency deviations and maintaining grid stability under nonlinear operating conditions. Furthermore, the CFOA demonstrates marginally superior convergence and tuning accuracy relative to the widely adopted Particle Swarm Optimization (PSO) algorithm. These findings underscore the proposed controller's potential as a high-performance solution for real-world LFC systems, particularly in scenarios characterized by nonlinearities and interconnected grid complexities. This study advances the field by bridging the gap between fractional-order fuzzy control theory and practical power system applications, offering a validated strategy for enhancing grid resilience in dynamic environments.

Keywords: LFC; dual-area power system; fuzzy FOPID + PI; CFOA; PSO; ITAE

check for updates

Academic Editors: Youssef Errami, Abdellatif Obbadi and Sahnoun Smail

Received: 18 May 2025
Revised: 23 June 2025
Accepted: 27 June 2025
Published: 28 June 2025

Citation: Almutairi, S.; Anayi, F.; Packianather, M.; Shouran, M. An Innovative LFC System Using a Fuzzy FOPID-Enhanced via PI Controller Tuned by the Catch Fish Optimization Algorithm Under Nonlinear Conditions. *Sustainability* **2025**, *17*, 5966. https://doi.org/10.3390/su17135966

1. Introduction

Load frequency control (LFC) is a critical component in the design and operational management of stable and reliable power systems. Inherently, power systems are subject to dynamic and stochastic load variations, which introduce uncertainties that adversely impact system frequency stability [1]. Such deviations from nominal frequency values are undesirable, as they compromise grid reliability and power quality. To mitigate these challenges, LFC mechanisms are employed to regulate frequency by dynamically adjusting generation output or minimizing frequency deviations, thereby maintaining system parameters within predefined operational thresholds. This regulatory process, referred to as load frequency control (LFC), is integral to ensuring the robustness and efficiency of modern power networks [2].

An optimally designed and effectively operated power system must demonstrate resilience against load disturbances while delivering an economically viable and high-quality power supply. LFC not only enhances transient and steady-state stability but also ensures compliance with operational constraints, balancing generation–demand mismatches and sustaining frequency within acceptable limits. Consequently, LFC serves as a foundational framework for achieving operational reliability, economic dispatch, and adherence to performance standards in power system engineering [3].

1.1. Literature Review

The escalating complexity and evolving dynamics of contemporary power systems have positioned load frequency control (LFC) as a pivotal mechanism for preserving grid stability and operational reliability. Over recent decades, an extensive volume of scholarly work has been devoted to the domain of LFC in interconnected power networks. LFC functions as a key control strategy to mitigate the detrimental impacts of load fluctuations on system frequency and tie-line power flow, thereby ensuring reliable system operation [4]. To confront these challenges, numerous control methodologies—ranging from conventional linear controllers to advanced intelligent techniques—have been explored to formulate resilient LFC frameworks capable of improving both transient performance and steady-state precision. Nevertheless, selecting the most appropriate LFC approach remains a complex endeavor, as each control scheme entails specific merits and drawbacks influenced by system nonlinearity, operational limitations, and regulatory conditions. Consequently, the practical realization of effective LFC systems demands in-depth domain expertise to navigate the inherent trade-offs between control complexity, flexibility, and performance robustness under dynamically varying grid environments [5,6].

The proportional–integral–derivative (PID) controller continues to serve as a fundamental component in LFC system design, primarily due to its structural simplicity, straightforward implementation, and well-established effectiveness in handling linear dynamics. Its widespread adoption extends far beyond power systems, with extensive use in industrial automation, robotics, and process control, reflecting its adaptability across engineering domains [7]. Within LFC applications, the PID controller maintains system frequency by modulating generator output based on proportional, integral, and derivative error components. In Ref. [8], a PI controller was optimized using the Flood Algorithm (FLA) for a two-area power system that integrates thermal and photovoltaic (PV) generation. The findings indicated that the FLA-optimized controller outperformed alternative metaheuristic approaches in terms of reduced settling time, minimal overshoot, and lower steady-state error, particularly under fluctuating solar input and variable load profiles. Similarly, the Firefly Algorithm (FA) was employed in Ref. [9] to fine-tune a PI controller for frequency regulation in a two-area system with PV integration. In another instance, Particle Swarm Optimization (PSO), a widely adopted technique, was applied in Ref. [10] to tune a PID controller in a stand-alone multi-source configuration for frequency control. Furthermore, the Artificial Bee Colony (ABC) algorithm was utilized in Ref. [11] to optimize PID parameters for an LFC scheme implemented in a hydro–thermal interconnected system. This controller outperformed conventional PID controllers tuned using different algorithms, including the Chef-Based Optimization Algorithm (CBOA) and Sine–Cosine Algorithm (SCA). In Ref. [12], the Lozi map-based Chaotic Optimization Algorithm (LCOA) was used to optimize parameters for a classical PID controller in a two-area interconnected power system for LFC. Furthermore, Ref. [13] proposed a Rat Swarm Optimization (RSO)-based PID controller demonstrating improved stability, shorter settling time, and near-zero frequency deviations. This method surpassed traditional approaches by consistently maintaining frequency regulation under dynamic conditions, strengthening overall system resilience.

Recent studies confirm that conventional PID controllers fundamentally struggle to mitigate the nonlinearities, parametric uncertainties, and communication delays inherent in modern power grids. To overcome these limitations, researchers have developed advanced variants including fractional-order PID (FOPID), PID-Acceleration (PIDA), and Filtered/Double-Derivative PID (PIDF/PIDD), alongside cascaded structures like PID-PI and adaptive gain-scheduled architectures.

Fractional-order PID (FOPID) controllers incorporate non-integer-order differentiation and integration operators through fractional calculus, enabling enhanced tuning flexibility and robustness. Recent advances confirm significant FOPID performance improvements in power systems. Specifically, Ref. [14] introduced optimized PID and FOPID controllers for load frequency control (LFC) in a three-area thermal–wind–hydro system, utilizing advanced metaheuristics—the Genetic Algorithm (GA), the Grey Wolf Optimizer (GWO), the Sine–Cosine Algorithm (SCA), and Atom Search Optimization (ASO)—with evaluation across multiple cost functions. The results demonstrated that ASO-tuned FOPID delivered superior transient performance and robustness under dynamic conditions. Complementarily, Ref. [15] developed an FOPID controller for single-area LFC, tuned via Integral Error Criterion (IEC) and applied to distinct turbine configurations: non-reheat, reheat, and hydro turbines. The controller was tuned for robustness against $\pm 50\%$ parameter uncertainties and demonstrated superior disturbance rejection relative to traditional approaches. Simulation outcomes validated the FOPID controller's capability to maintain performance under both nominal and uncertain system conditions. Concurrently, Ref. [16] introduced a deregulated hybrid power system scenario in which an Aquila Optimizer (AO)-based FOPID controller was developed for LFC. Comparative analysis showed that the AO-FOPID configuration outperformed controllers optimized using Particle Swarm Optimization (PSO) and the Whale Optimization Algorithm (WOA), effectively reducing frequency deviations and tie-line power oscillations across a range of dynamic operating conditions.

Regarding PID-Acceleration (PIDA), Ref. [17] developed hybrid strategies combining Teaching–Learning-Based Optimization (TLBO), Tabu Search (TS), and Equilibrium Optimizer (EDO) for PIDA tuning in two-area load frequency control. These methods enhanced convergence speed, dynamic response, and robustness against load variations and renewable energy fluctuations. The simulation results demonstrated that the TLBO-EDO-tuned PIDA controller outperformed conventional methods by minimizing peak-to-peak oscillations, root mean square (RMS) error, and tie-line power deviations under multiple contingencies. Regarding Filtered/Double Derivative PID (PIDF/PIDD), n Ref. [18], a Modified Whale Optimization Algorithm (MWOA) was proposed to tune a proportional–integral–derivative with filter (PIDF) controller for load frequency control in a two-area photovoltaic–thermal power system. The simulation results demonstrated that the MWOA-optimized PIDF controller delivered improved damping characteristics and enhanced robustness compared to controllers tuned using conventional optimization techniques. In a separate study [19], a proportional–integral–double-derivative (PIDD) controller was applied to an isolated hybrid power system (IHPS) comprising conventional generators, renewable energy sources, energy storage devices, and electric vehicles (EVs). The controller parameters were optimized using the Magneto-Tactic Bacteria Optimization (MBO) algorithm, with tuning guided by a peak-based integral square error (PISE) performance index. The simulation results indicated that the PIDD controller provided superior frequency regulation under combined load and generation disturbances, outperforming classical counterparts. However, nonlinearities, such as generation rate constraints and governor dead band, were not included in the control design. These variants attenuated high-frequency noise sensitivity while enhancing transient performance, with PIDD structures demonstrating superior robustness under load variations.

However, PID-based controllers require precise tuning and demonstrate limited effectiveness in highly nonlinear or stochastic environments. These limitations have motivated the development of advanced control methodologies aimed at overcoming the constraints of linear controller architectures:

- Sliding Mode Control (SMC): SMC is recognized for its robustness against uncertainties, directing system trajectories toward a predefined sliding surface. Recent studies on SMC for load frequency control (LFC) have introduced various advanced controller designs and optimization strategies. In Ref. [20], an SMC design was developed for a simplified model of the Great Britain power system, utilizing a five-parameter sliding surface optimized through the Bees Algorithm (BA) and Particle Swarm Optimization (PSO), with performance evaluated using the ITAE criterion. The results were compared to a BA-tuned PID controller, showing that the SMC configuration delivered a superior dynamic response and stronger robustness to parameter uncertainties. In Ref. [21], an output feedback SMC was proposed for a multi-area, multi-source power system, where Teaching–Learning-Based Optimization (TLBO) was used to tune feedback gains and switching vectors. This design outperformed other approaches based on Differential Evolution, PSO, and Genetic Algorithms and included consideration of HVDC link dynamics. The study in Ref. [22] developed a four-parameter SMC controller optimized by PSO and Grey Wolf Optimization (GWO), implemented across single-, two-, and four-area systems. It demonstrated significant improvements in frequency regulation and robustness under load disturbances and system uncertainties. While all three works emphasized robust controller tuning under various disturbance scenarios, none explicitly incorporated nonlinear dynamics into the system models.
- Linear Quadratic Regulator (LQR): The studies in Refs. [23,24] proposed LQR-based approaches for load frequency control in power systems but omitted nonlinear considerations during controller design. In Ref. [23], an advanced LQR scheme based on Linear Matrix Inequalities (LMIs) was implemented in a hybrid system incorporating wind turbines, diesel generators, fuel cells, aqua-electrolyzes, and battery energy storage. This controller exhibited improved performance under various disturbances when compared with conventional closed-loop LQR methods. In Ref. [24], the LQR technique was applied to a two-area power system and assessed against a conventional PI controller under step load perturbations, with evaluation focusing on frequency regulation and system stability. While both studies demonstrated the effectiveness of optimal control strategies in enhancing LFC performance, they were constrained by their reliance on linearized models, limiting their applicability to real-world systems characterized by inherent nonlinear dynamics.
- Model Predictive Control (MPC) techniques enhance LFC performance under diverse operating conditions. In Ref. [25], a hybrid Grey Wolf Optimizer–Pattern Search (HGWO–PS)-tuned MPC for a two-area islanded microgrid was used to improve frequency stability and reduce control complexity.
- Adaptive control strategies for LFC in interconnected power systems were proposed in Refs. [26,27] to enhance stability under disturbances and parameter variations. Specifically, Ref. [26] introduced an adaptive PI controller that dynamically tuned gains during load/renewable fluctuations (including WECS and PV–thermal systems), exhibiting superior robustness and transient performance versus conventional

PI/optimized PID methods. In contrast, Ref. [27] implemented decentralized Model Reference Adaptive Control (MRAC) for two-area systems, utilizing local feedback signals with Lyapunov-based stability guarantees. Critically, both approaches neglected nonlinear elements (dead bands, valve limits), potentially compromising real-world applicability and reliability.

➢ H-infinity Control (H∞): The study in Ref. [28] proposed a robust H∞-based LFC strategy for a two-area interconnected power system, addressing nonlinearities and parameter uncertainties using a sector-bounded formulation. The simulation results confirmed superior performance compared to conventional PI controllers, with reduced frequency deviations and enhanced stability under load disturbances and uncertainty. The method further demonstrated scalability to multi-area systems while sustaining robust performance across varying operating conditions.

Fuzzy Logic Control (FLC) offers a potent solution for LFC in nonlinear, stochastic, and model-agnostic environments by leveraging expert-defined linguistic rules for decision-making under uncertainty. Its key advantages include intrinsic nonlinearity handling [29], enhanced robustness [30], and compatibility with hybrid architectures [31,32]. However, FLC performance critically depends on the rule base and membership function design, demanding rigorous optimization that may challenge practical implementation. Table 1 summarizes LFC systems reported in the literature.

Table 1. LFC systems proposed in the literature.

Ref.	Year	Control Method	Optimization Tool	Renewable Energy	Nonlinear Elements	Nonlinearity Impact Investigation
[8]	2025	PI	FLA	✓	×	×
[9]	2018	PI	FA	✓	×	×
[10]	2023	PID	PSO	×	×	×
[11]	2022	PID	ABC	×	×	×
[12]	2012	PID	LCOA	×	×	×
[13]	2024	PID	RSO	×	×	×
[14]	2023	PID/FOPID	ASIA	✓	×	×
[15]	2014	FOPID	IEC	×	×	×
[16]	2024	FOPID	AO	×	×	×
[17]	2025	PIDA	TLBO	×	×	×
[18]	2020	PIDF	MWOA	✓	×	×
[19]	2024	PIDD	MBO	✓	×	×
[20]	2022	SMC	BA	×	×	×
[21]	2015	SMC	TLBO	×	×	×
[22]	2021	SMC	GWO	×	×	×
[23]	2013	LQR	-	×	×	×
[24]	2024	LQR	-	✓	×	×
[25]	2023	MPC	HGWO–PS	×	×	×
[26]	2022	Adaptive PI	-	✓	×	×
[27]	2021	MRAC	-	×	×	×
[28]	2016	H∞	-	×	×	×
[29]	2022	Fuzzy PID	WCA	✓	✓	×
[30]	2016	Hybrid Fuzzy	PSO	×	×	×
[31]	2023	Hybrid Fuzzy	DE and GA	✓	✓	×
[32]	2022	Several hybrid Fuzzy structures	BA	×	×	×

Concisely, classical PID controllers remain a cornerstone of LFC because of their simplicity and cost-efficiency. Yet, their limited effectiveness under nonlinear and uncertain conditions necessitates the adoption of advanced control strategies:

- ➢ Enhanced PID variants—such as FOPID and PIDA—extend classical PID capabilities in robustness and adaptability, though at the cost of increased design and tuning complexity.
- ➢ Advanced controllers (SMC, MPC, H∞) provide precision and robustness but encounter computational and implementation challenges.
- ➢ Fuzzy Logic Control balances adaptability and implementation feasibility in hybrid architectures, positioning it as a viable strategy for modern power systems.

1.2. Objectives and Contributions

A critical gap remains in evaluating how nonlinearities, specifically generation rate constraints (GRCs) and governor dead band (GDB), influence frequency stability within load frequency control (LFC) systems. While prior work acknowledges their operational significance, few studies rigorously assess their impact when integrated into or excluded from LFC design. This underscores the need for a systematic investigation into how these elements affect LFC performance and overall system dynamics. This study conducts a comprehensive analysis of GRC and GDB effects on frequency regulation, addressing a pivotal research gap.

1.2.1. Challenges in LFC System Design

A core challenge in LFC design lies in balancing rapid dynamic response with system stability. Fast transient correction enables timely frequency stabilization in dynamic grids, particularly during load fluctuations, thereby minimizing downtime and maintaining operational continuity. However, aggressive responses risk overshoots that exceed safety thresholds, jeopardizing sensitive equipment. In contrast, slower corrections ensure frequency adherence but may introduce underfrequency or overfrequency deviations during transitions, reducing reliability. Thus, optimal LFC controllers must harmonize rapid stabilization with overshoot minimization to ensure both performance and operational safety.

1.2.2. Limitations of Existing Control Strategies

Traditional PID controllers remain prevalent in LFC applications because of their simplicity, cost-efficiency, and ease of implementation. However, their performance deteriorates in the presence of nonlinearities, parametric uncertainties, and system sensitivity—challenges typical of modern power networks. Notably, PID controllers often struggle to maintain voltage stability during dynamic load variations. Advanced methods, such as adaptive control and Sliding Mode Control (SMC), offer improved robustness. Adaptive control adjusts gains in real time, enhancing performance under uncertainty, though its complexity and tuning demands limit practical deployment. SMC provides robustness against matched uncertainties but introduces chattering—undesired high-frequency oscillations that impair performance and accelerate actuator wear. Fuzzy logic controllers (FLCs) eliminate the need for precise mathematical models by utilizing expert-defined linguistic rules. Nevertheless, many FLC implementations overlook robustness under variable operating conditions, limiting their reliability in dynamic environments.

1.2.3. Proposed Methodology and Contributions

This study proposes a novel hybrid fuzzy controller that integrates a fuzzy fractional-order proportional–integral–derivative (FOPID) structure with a classical PI controller, optimized using the Catch Fish Optimization (CFO) algorithm. The main contributions are outlined as follows:

1. Impact of Nonlinear Elements: This study conducts a systematic investigation of GRCs and GDB on power system stability, providing critical insights for future LFC design.

2. Innovative Controller Design: This study proposes a hybrid FOPID + PI configuration that synergizes fuzzy logic adaptability with classical control precision to enhance stability and dynamic response.
3. Optimization via Metaheuristic Algorithms**:** The CFO algorithm is applied for the first time in LFC contexts to optimize controller parameters, complemented by Particle Swarm Optimization (PSO) for comparative validation.
4. Comprehensive Performance Evaluation: This study conducts a rigorous comparative analysis against existing controllers, demonstrating superior transient response, overshoot mitigation, and robustness under parametric uncertainties. Also, the proposed controller is implemented in two different power systems under different operating conditions to validate its readiness for real-time operation.
5. Robustness Validation: The proposed controller exhibits resilience in maintaining frequency stability under diverse disturbances, including $\pm35\%$ parametric variations and abrupt load changes.

By integrating fractional-order dynamics with fuzzy logic and metaheuristic optimization, this study advances LFC controller design, addressing the limitations of conventional and advanced methods. The hybrid Fuzzy FOPID + PI controller demonstrates enhanced reliability, robustness, and adaptability in dynamic environments, offering a viable solution for modern power systems. These findings underscore the imperative of incorporating nonlinear element analysis and innovative control architectures to ensure stable, efficient frequency regulation in increasingly complex grids.

1.3. Paper Structure

The organizational structure of this research paper is delineated as follows: Section 2 establishes a mathematical framework for the power systems under investigation, incorporating parameter specifications and rigorously defining the nonlinear elements central to the analysis, namely, GRCs and GDB. Section 3 elaborates on the innovative architecture of the proposed LFC mechanism, accompanied by a systematic exposition of the optimization methodologies employed and the formulation of the objective function governing the design process. Section 4 presents an empirical validation of the proposed framework, offering a critical analysis of the results derived from diverse operational scenarios to underscore the methodological robustness and comparative efficacy of the approach. Moreover, it conducts a rigorous robustness assessment of the FLC based on the CFOA, examining its performance under different parametric uncertainty scenarios. Finally, Section 5 synthesizes the principal findings of this study, articulates their theoretical and practical implications, and proposes trajectories for subsequent research endeavors to address unresolved challenges and extend the applicability of the proposed framework.

2. Power Systems Under Study: Modeling and Parameters

This study conducts a comparative analysis of two distinct power systems to evaluate the practical efficacy of the proposed fuzzy control framework. The first system is employed to investigate the influence of governor dead band (GDB) nonlinear dynamics on operational stability, while the second system is utilized to assess the effects of generation rate constraint (GRC) nonlinear characteristics on power system stability. These case studies collectively demonstrate the robustness of the control architecture in addressing nonlinear constraints inherent to modern power grid operations.

2.1. Power System One

This section analyses a widely recognized two-area power system model, a benchmark configuration extensively validated in power grid stability research. The system comprises two asymmetrically parameterized interconnected regions, integrated with standard components, such as governors, turbines, load dynamics, and synchronous machines, to emulate real-world operational conditions. The schematic of the testbed architecture is illustrated in Figure 1, with comprehensive parameter specifications enumerated in Appendix A [33]. Central to the design of load frequency control (LFC) frameworks is the area control error (ACE), a foundational feedback metric that quantifies system-level imbalances. The ACE synthesizes both frequency deviation and tie-line power exchange discrepancies, establishing the core inputs for the LFC controller's corrective actions. Within the examined two-area framework, the ACE for areas 1 and 2 is formally expressed through Equations (1) and (2), respectively, enabling precise frequency regulation under dynamic load variations.

$$\mathrm{ACE}_1 = \Delta \mathrm{P}_{12} + \mathrm{B}_1\, \Delta \mathrm{F}_1 \tag{1}$$

$$\mathrm{ACE}_2 = \Delta \mathrm{P}_{21} + \mathrm{B}_2\, \Delta \mathrm{F}_2 \tag{2}$$

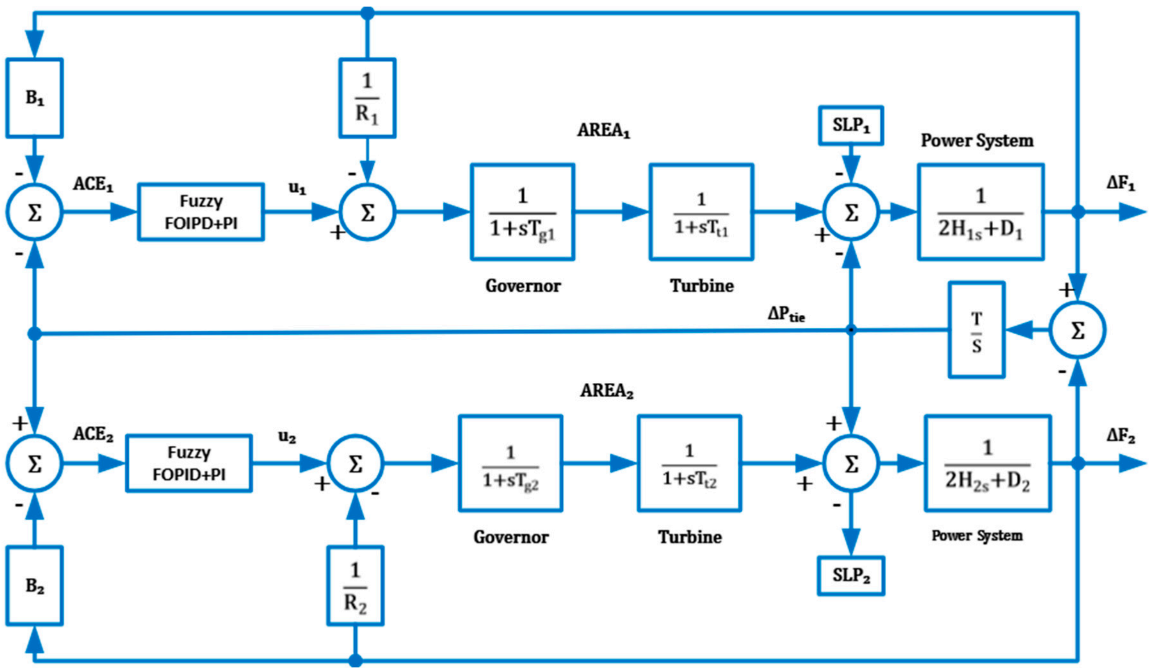

Figure 1. The first power system under study.

The variables ΔF_1 and ΔF_2 represent frequency deviations in areas 1 and 2, ΔP_{12} and ΔP_{21} indicate tie-line power flow deviations, and B_1 and B_2 are the respective frequency bias coefficients for each area.

2.2. Governor Dead Band (GDB) Modeling and Integration

Governor dead band (GDB) constitutes an inherent physical nonlinearity in power system governor mechanisms, characterized by a defined threshold range within which minor frequency deviations fail to elicit a corrective response from the governor valve. This phenomenon originates from two primary factors: (i) inherent mechanical tolerances in the valve positioning system, which introduce operational slack, and (ii) deliberate signal filtering implemented to mitigate excessive control actuations caused by transient disturbances. The resultant latency in governor response compromises the efficacy of LFC systems by inducing phase lag, amplifying power oscillations, and diminishing regulation precision.

To accurately emulate real-world turbine–governor dynamics, the GDB nonlinearity is integrated into the system model, implemented in accordance with the analytical framework established by Ref. [34]. This formulation explicitly accounts for the governor valve's non-responsive zone during small-magnitude speed variations. The modified governor transfer function incorporating GDB effects is expressed as:

$$G_{GDB}(s) = \frac{-\frac{0.2}{\pi}s + 0.8}{T_g s + 1} \tag{3}$$

where T_g denotes the governor time constant. The coefficients 0.8 and $-\frac{0.2}{\pi}$ in the numerator quantitatively characterize the dead band's asymmetric influence on valve displacement dynamics, as rigorously derived in Ref. [34]. This nonlinear element is intentionally embedded within the governor block architecture of the system presented in Figure 1 to systematically assess controller performance under non-ideal operational constraints, thereby validating robustness against realistic electromechanical disturbances.

2.3. Power System Two

To evaluate the practical feasibility of the proposed control strategy, the controller is integrated into two distinct experimental testbed systems, thereby enhancing the realism and robustness of the assessment while providing empirical validation of the paradigm's efficacy. As depicted in Figure 2, the second testbed system comprises a two-area interconnected power grid integrated with a non-reheat thermal generation unit. The system's critical parameters, such as nominal frequency (F_i, Hz), regulation coefficient (Ri, Hz/unit), speed governor time constant (T_{gi}, s), turbine time constant (T_{ti}, s), and power system time constant (T_{pi}, s), are rigorously defined to reflect operational dynamics. The model further integrates key dynamic components, including area control error (ACE_i), load demand perturbation (ΔP_{Di}), speed changer positional adjustment (ΔP_{ci}), governor valve displacement (ΔP_{gi}), power system gain (K_{Pi}), and tie-line power exchange deviation (ΔP_{tie}). A comprehensive summary of these parameters and their corresponding values is provided in Appendix B [35].

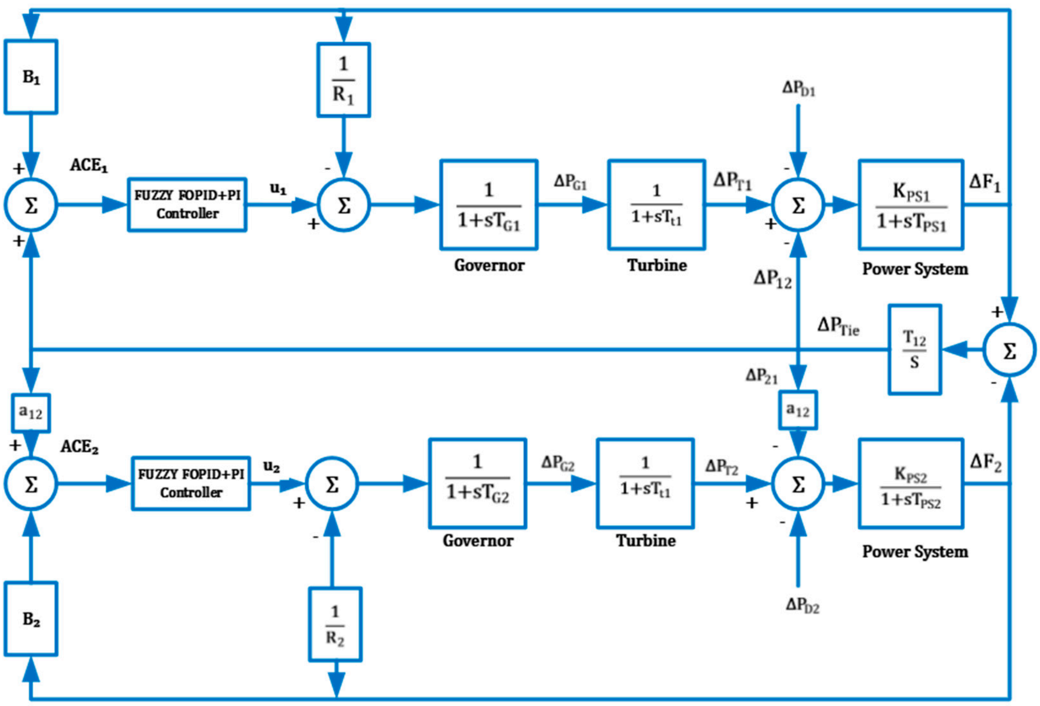

Figure 2. The second power system under study.

2.4. Generation Rate Constraint (GRC) Modeling and Integration

The generation rate constraint (GRC) refers to the physical limitation on the rate at which a power-generating unit can increase or decrease its output. These constraints arise because of the inherent thermal dynamics, mechanical inertia, and safety considerations of the turbine system. The GRC is typically expressed as upper and lower bounds on the rate of change in the turbine output, ensuring that the unit operates within safe and realistic operational margins. Ignoring GRCs in dynamic simulations can result in unrealistically fast power adjustments that do not reflect the behavior of actual power plants.

To account for this practical limitation, the linear non-reheat turbine model depicted in Figure 2 is replaced with a nonlinear representation shown in Figure 3, which explicitly incorporates GRCs bounded at ($\alpha = \pm 0.025$) per unit per second. This nonlinear model includes a saturation function that enforces rate limits on the turbine's power response, effectively capturing the delayed behavior caused by physical inertia and thermal lag. As highlighted in Ref. [35], this modeling approach ensures that turbine output changes adhere to feasible dynamic trajectories, avoiding artificial performance gains in simulation studies.

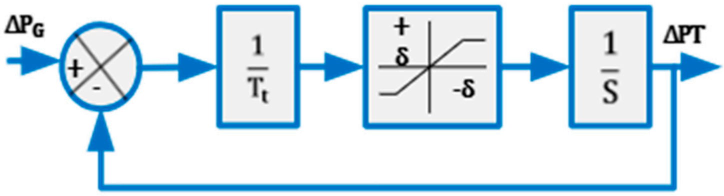

Figure 3. Nonlinear turbine model with GRCs.

Moreover, as emphasized in Ref. [36], incorporating GRCs is crucial for accurately assessing the performance of load frequency control strategies. Its omission can lead to overly optimistic evaluations of controller response times and stability. By integrating GRCs directly into the turbine block, the model provides a more realistic and credible framework for analyzing system frequency behavior and tie-line power exchanges under dynamic conditions.

3. The Proposed Controller and Tuning Tool

3.1. The Fuzzy FOPID Enhanced by Classical PI

Figure 4 illustrates the architecture of the proposed hybrid control strategy, integrating three core components: a fuzzy logic controller (FLC), a fractional-order proportional–integral–derivative (FOPID) controller, and a conventional proportional–integral (PI) controller. The FLC is configured with two normalized input variables—the ACE and its derivative $\dot{ACE}$—scaled via gains K_1 and K_2, respectively. A single output signal generated by the FLC serves as the input to the FOPID controller.

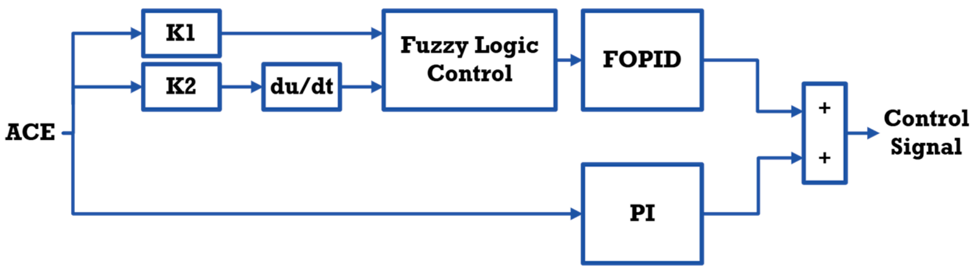

Figure 4. The configuration of the proposed LFC system.

To optimize computational efficiency and ensure real-time applicability, the FLC employs triangular membership functions (MFs) for fuzzification, with five linguistic categories assigned to both inputs and outputs, including Negative Big (NB), Negative Small (NS), Zero (Z), Positive Small (PS), and Positive Big (PB), as depicted in Figure 5. A rule base of 25 expert-defined fuzzy rules (Table 2 governs the inference system, formulated to align with the dynamic behavior of the target system. The Mamdani inference mechanism is utilized for mapping crisp inputs to fuzzy sets, while defuzzification is executed via the centroid method to produce a deterministic control signal.

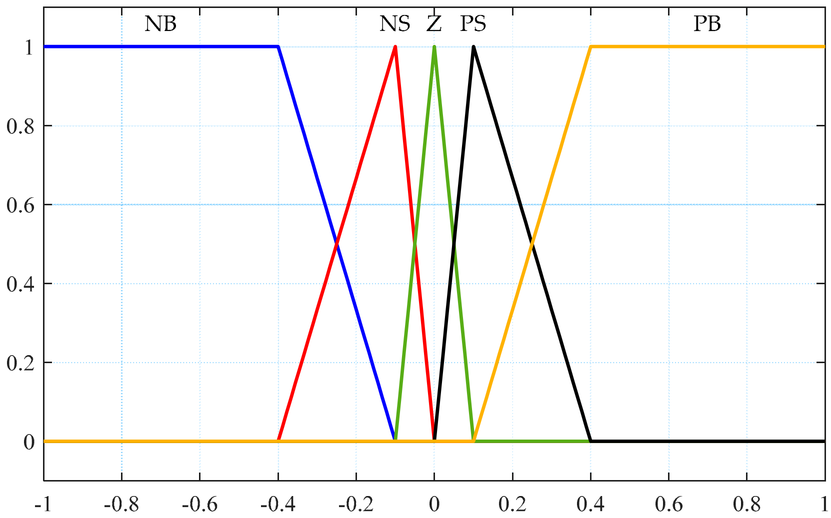

Figure 5. The membership functions of the fuzzy controller.

Table 2. The rule base of the FLC component.

Error	Change of Error				
	NB	**NS**	**Z**	**PS**	**PB**
NB	NB	NB	NB	NS	Z
NS	NB	NB	NS	Z	PS
Z	NB	NS	Z	BS	PB
PS	NS	Z	PS	PB	PB
PB	Z	PS	PB	PB	PB

The FOPID controller extends the classical PID framework by incorporating fractional-order operators for integration (λ) and differentiation (μ), enhancing adaptability to complex system dynamics. Its transfer function is expressed as:

$$\mathrm{FOPID\ Controller_c(S)} = K_{P1} + K_{I1}S^{-\lambda} + K_{D1}S^{\mu} \tag{4}$$

where $K_{P1}, K_{I1}, \mathrm{and} K_{D1}$ denote proportional, integral, and derivative gains, respectively, while λ and μ represent the fractional orders. Concurrently, a parallel PI controller processes the same error signal, with its transfer function defined as:

$$\mathrm{PI\ Controller_c(S)} = K_{P2} + \frac{K_{I2}}{S} \tag{5}$$

The hybrid control action is synthesized by aggregating the outputs of the Fuzzy FOPID and PI controllers. This synergistic integration leverages the FLC's nonlinear adaptability, the FOPID's extended tuning flexibility, and the PI controller's steady-state precision, collectively achieving superior dynamic response, robust disturbance rejection, and high-accuracy trajectory tracking under heterogeneous operating conditions.

The proposed hybrid controller addresses intractable load frequency control challenges nonlinear dynamics, parametric uncertainties, and rapid disturbance rejection requirements in interconnected power systems. Its fuzzy logic layer dynamically adjusts control gains through real-time error mapping, enabling adaptive compensation during transients. The FOPID component enhances the transient response via fractional-order operators, providing superior tuning flexibility and memory-effect approximation over classical PID. Parallel PI action guarantees steady-state error elimination. Fuzzy rules are synthesized from system responses to step-load perturbations, capturing both large-signal and small-signal behaviors. Triangular membership functions and Mamdani inference ensure computationally efficient implementation while preserving expressive control logic.

3.2. The Suggested Tuning Tool: Catch Fish Optimisation Algorithm

The Catch Fish Optimization Algorithm (CFOA) is a novel, human behavior-inspired metaheuristic algorithm that emulates traditional fishing strategies employed in rural settings. It combines the principles of independent search, group collaboration, and collective encirclement to balance global exploration and local exploitation within an optimization process [37]. The CFOA is particularly suited for solving complex nonlinear problems and is adopted in this study to optimally tune the parameters of the proposed fuzzy controller for LFC in power systems. The CFOA's selection is further supported by its demonstrated success in solving complex, nonlinear, and high-dimensional problems in other domains, such as enhancing surface quality and microhardness in laser cladding processes [38] and achieving stable convergence in solar thermal system optimization under uncertainty [39], validating its robustness and global search efficacy for LFC design.

Mechanism and Design Philosophy

CFOA operates through two main phases:

Exploration Phase: The exploration phase simulates early fishing behavior, where individual "fishermen" (search agents) disturb the water to locate fish independently and later collaborate in small groups to encircle fish-rich zones. This phase allows for extensive global search capabilities.

Exploitation Phase: The exploitation phase resembles a coordinated collective encirclement, where all agents converge strategically toward the best-known solution. A Gaussian distribution is used to model agent positioning, encouraging convergence to the global optimum while maintaining diversity.

These mechanisms are dynamically managed using a capture rate parameter that transitions agents from exploratory to exploitative behaviors as iterations progress.

Algorithm Workflow

The Catch Fish Optimization Algorithm (CFOA) is conceptually grounded in the core behavioral patterns of traditional fishing practices. Following a concise exposition of its theoretical basis, the algorithm's essential operational procedures are comprehensively delineated [37]. The CFOA operates through two principal stages: the exploration phase, which entails cooperative fishing behavior and spatially diversified search to maximize the identification probability of advantageous regions within the solution space, and the exploitation phase, defined by strategically coordinated encirclement that utilizes collective dynamics to intensify the search proximate to promising areas [37]. Throughout the optimization process, the algorithm sustains an adaptive global search strategy, wherein multiple agents—each representing an individual fisherman—dynamically adjust their positions within the defined search domain. This coordinated behavior enables effective equilibrium between diversification and intensification. The mathematical formulation governing this process is presented in Equation (6), with each fisherman functioning as an autonomous optimization agent.

$$\text{Fisher} = \begin{bmatrix} \text{Fisher}_{1,1} & \text{Fisher}_{1,2} & \ldots & \text{Fisher}_{1,d} \\ \text{Fisher}_{2,1} & \text{Fisher}_{2,2} & \ldots & \text{Fisher}_{2,d} \\ \vdots & \vdots & \ddots & \vdots \\ \text{Fisher}_{1,1} & \text{Fisher}_{1,2} & \ldots & \text{Fisher}_{1,d} \end{bmatrix} \text{N} \times \text{d} \tag{6}$$

Equation (7) represents Fisher's resetting formulation, which constitutes a comprehensive matrix mathematically encapsulating the positional coordinates of N search agents within a d-dimensional solution space.

$$\text{Fisher}_{i,j} = \left(\text{ub}_\text{j} - \text{lb}_\text{j}\right) \times \text{r} + \text{lb}_j \tag{7}$$

The upper and lower bounds of the j-th dimension are defined by ub_j and lb_j, the position of the i-th fisherman in the j-th dimension is denoted as $\text{Fisher}_\text{i.j}$, and r represents a stochastically generated value within the bounded interval [0, 2].

The fitness value assessment function$_\text{fobj}$ and current location data compute each fisherman's fitness. Equation (8) presents the resulting fitness value matrix.

$$\text{fit} = f_\text{objective}(\text{Fisher}) = \begin{bmatrix} \text{fit}_1 \\ \text{fit}_2 \\ \vdots \\ \text{fit}_N \end{bmatrix} \tag{8}$$

3.2.1. Exploration Phase (EFs/MaxEFs < 0.5)

The highest capture rates and maximal fish quantities occur during the initial fishing season; however, a progressive decline in fish availability correlates with reduced catch rates. Consequently, fishermen initially prioritize individual search strategies involving targeted seeking and hydrodynamic disruption to maximize yield. As the hunt progresses, fishermen gradually acquire environmental dominance over fish populations. This transition is characterized by increased aquatic turbulence and diminished fish discernibility. Sustained harvesting during the search operation depletes fish stocks and further reduces capture rates. When collective encirclement emerges as the dominant survival strategy, individual advantages become subordinate to collective imperatives. The parameter α, representing the capture rate, models this behavioral transition in Equation (9).

$$\alpha = \left(1 - \frac{3 \times \text{EF}_s}{2 \times \text{MaxEF}_s}\right)^{\frac{3\times\text{EF}_s}{2\times\text{MaxEF}_s}} \tag{9}$$

Evaluations are quantified as EFs (denoting current evaluation count) and MaxEFs (representing the maximum evaluation threshold). Fishermen autonomously select between collective capture and independent search strategies. When the capture rate α is elevated, individual search tactics are prioritized; conversely, reduced α values prompt a transition to collective capture. This behavioral shift is modeled using binary stochastic variables (0, 2), where p denotes a selection probability threshold and α represents a uniformly distributed random variable within the interval [0, 2]. Collective capture activation occurs when $\text{p} \geq \alpha$, while independent search initiation is triggered when $\text{p} < \alpha$.

During independent search ($\text{p} < \alpha$), fishermen generate hydrodynamic disturbances to induce aquatic turbidity, compelling fish to surface or release gas bubbles that manifest as detectable ripple patterns. Based on observed disturbance signatures and capture efficacy, fishermen dynamically refine their search trajectory, alternating between localized exploration and regional relocation as required. This position update mechanism is formalized in Equations (10) and (11):

$$\mathrm{Exp} = \frac{\mathrm{fit}_1 - \mathrm{fit}_p}{\mathrm{fit}_{\mathrm{maximum}} - \mathrm{fit}_{\mathrm{minimum}}}, \tag{10}$$

$$R = \mathrm{Dis} \times \sqrt{|\mathrm{Exp}|} \times \left(1 - \frac{\mathrm{EF_s}}{\mathrm{MaxEF_s}}\right), \tag{11}$$

$$\mathrm{Fisher}_{i,j}^{T+1} = \mathrm{Fisher}_{i,j}^{T} + \left(\mathrm{Fisher}_{pos,j}^{T} - \mathrm{Fisher}_{i,j}^{T}\right) \times \mathrm{Exp} + r_s \times s \times R. \tag{12}$$

The empirical evaluation metric Exp, bounded within the interval $(-1, 1)$, quantifies the significance of heuristic assessments derived by a fisherman when utilizing any posth fisherman (pos = 1, 2, . . . , N; $p \neq i$) as a reference target. Following the T-th complete position update cycle, fit_{min} and fit_{max} represent the optimal and poorest fitness values, respectively, where T denotes the cumulative count of positional adjustments executed. The coordinates $\mathrm{Fisher}^{T}{}_{i,j}$ and $\mathrm{Fisher}^{T+1}{}_{i,j}$ correspond to the j-dimensional position of the i-th fisherman at iterations T and T + 1. The stochastic parameter r_s is uniformly distributed within [0, 2], while Dis measures the Euclidean distance between the reference agent and the i-th fisherman. A d-dimensional stochastic unit vector is denoted by s.

The primary movement vector (indicating favorable guidance received from peer fishermen) and displacement magnitude are computed through statistical analysis, constrained by $R \leq \mathrm{Dis}$. Additionally, the exploration radius R is modulated by both the current evaluation count ($\mathrm{EF_s}$) and the absolute value of Exp.

During the exploration phase, the central agent exhibits bidirectional extension relative to a stochastically selected reference agent. The permissible displacement space is defined by an exploration radius R, representing the radial distance from the centroid of agent positions. This radius bounds the maximum allowable movement during position updates. One agent prepares for positional adjustment, while the reference agent remains fixed to serve as a coordination target. Movement directions are classified into three categories: approach vectors (indicating progression toward the reference), retreat vectors (indicating movement away), and lateral drift vectors (representing autonomous exploratory behavior). These coordinated and uncoordinated movement modes enable the algorithm to balance global exploration with local refinement.

Fishermen collectively coordinate in cohorts of three or four agents to encircle candidate prey concentrations during group capture ($p \geq \alpha$), deploying net-based strategies to maximize yield. Movement vectors (direction and displacement magnitude) are modulated by environmental conditions, inter-agent relationships, and fitness states. As capture success increases and agent density intensifies, positional adjustments exhibit progressive refinement in precision. The operational logic underlying this group coordination behavior is formally represented by the mathematical model in Equations (13) and (14).

$$\mathrm{Centre}_c = \mathrm{mean}\left(\mathrm{Fisher}_c^T\right), \tag{13}$$

$$\mathrm{Fisher}_{c,i,j}^{T+1} = \mathrm{Fisher}_{c,i,j}^{T} + r_2\left(\mathrm{Centre}_c - \mathrm{Fisher}_{c,j}^{T}\right) + \left(1 - \frac{2 \times \mathrm{EF_s}}{\mathrm{MaxEF_s}}\right) \times r_3. \tag{14}$$

The group c comprises three or four agents that maintain fixed positional assignments. The centroid point, denoted as Centre_c, serves as the central objective for the collective encirclement behavior of group c. Following the T-th and (T + 1)-th update cycles, $\mathrm{Fisher}_{c,i,j}^{T}$ and $\mathrm{Fisher}_{c,i,j}^{T+1}$ denote the j-dimensional coordinates of the i-th fisherman within group c.

The convergence pace toward the centroid, represented by r_2, exhibits stochastic variation across agents within the interval [0, 2]. The displacement offset parameter r_3 takes values within the range $[-1, 1]$ and gradually contracts as the number of evaluation counts (EF_s) increases.

The resulting displacement vector defines the fisherman's updated movement magnitude and direction in two-dimensional space.

3.2.2. Exploitation Phase (EFs/MaxEFs $\geq$ 0.5)

Throughout the harvesting process, partial fish evasion occurs, yet fishermen collectively execute driving and encircling maneuvers to contain fugitive specimens. Agents are strategically deployed surrounding the prey concentration, with centrally positioned units focusing on the primary school while peripheral agents intercept escaping individuals. This cooperative configuration enhances capture efficiency. The spatial distribution is modeled according to a Gaussian framework, with the formalized mathematical representation provided in Equations (15) and (16):

$$\sigma = \sqrt{\left(2\left(1 - \frac{EF_s}{MaxEF_s}\right) / \left(1 - \frac{EF_s}{MaxEF_s}\right)^2 + 1\right)}. \tag{15}$$

$$\mathrm{Fisher}_i^{T+1} = G_{\mathrm{best}} + \mathrm{GD}\left(0, \frac{r_4 \times \sigma \times |\mathrm{Fisher} - G_{\mathrm{best}}|}{3}\right) \tag{16}$$

where GD represents the Gaussian distribution function. The variance parameter σ increases with the evaluation count, transitioning from 0 to 2, while the mean μ remains fixed at 0. The centroid position across all dimensions is mathematically represented as a matrix corresponding to the i-th fisherman's coordinates after the (T + 1)-th update cycle. The global optimum solution (Gbest), which serves as the global reference point for positional updates, is used as a target during exploitation. Fishermen are partitioned into three distinct spatial regions determined by r_4, a discrete stochastic variable with possible values {1, 2, 3}.

3.2.3. Implementation Process of the CFOA

The search mechanism diverges from conventional Particle Swarm Optimization (PSO) through the stochastic selection of distinct regions for comparative scenario evaluation. When encountering comparable fitness between independently explored and newly evaluated regions, the algorithm maintains its current search domain. Upon identifying superior fitness elsewhere, it inversely explores peripheral zones; conversely, inferior fitness triggers relocation to alternative regions. Local exploration occurs via coordinated encirclement, while individual search transitions to collective mode based on capture rate thresholds. This dual-strategy approach enhances global search comprehensiveness and efficacy. Final refinement of the optimal solution is achieved through iterative collective capture. The CFOA principally emphasizes two interconnected optimization phases: exploratory diversification and exploitative intensification. The complete procedural logic is illustrated in the flowchart in Figure 6.

In this work, the CFOA was used to optimize the proposed fuzzy control gains designed for LFC in a multi-area power system. The optimization objective was to minimize the Integral Time Absolute Error (ITAE) objective function of the ACE, as expressed in Equation (17), following a disturbance.

$$\mathrm{ITAE}_{\text{Objective function}} = |\Delta \mathrm{F}_1| + |\Delta \mathrm{F}_2| + |\Delta \mathrm{P}_{12}|.\mathrm{t}\ .\mathrm{dt} \tag{17}$$

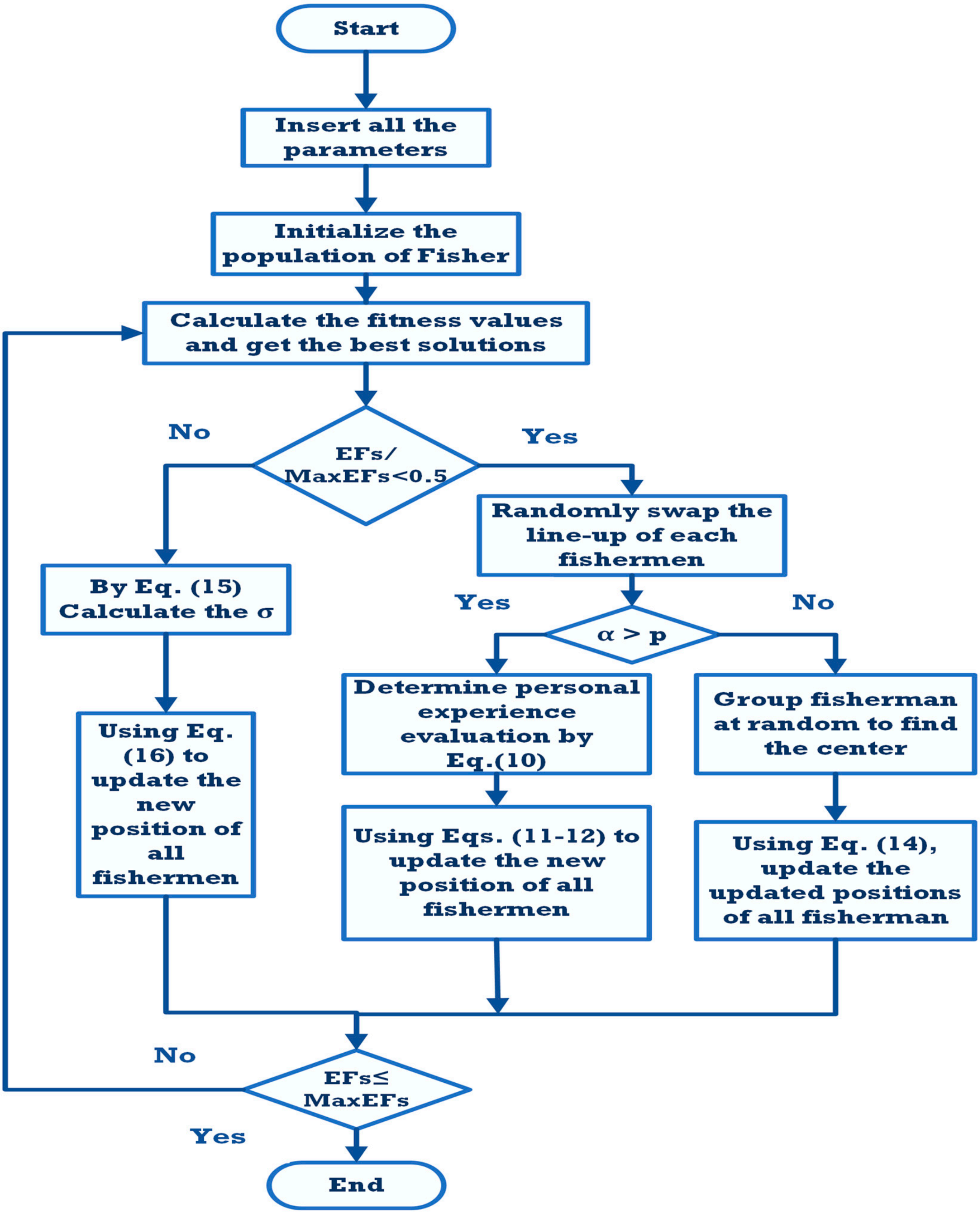

Figure 6. The flowchart of the Catch Fish Optimization Algorithm.

The CFOA ensured faster convergence to optimal controller parameters, better disturbance rejection, and reduced frequency overshoot and settling time compared to classical tuning methods.

The main advantages of the CFOA in LFC tuning include the following:

Balanced Search Strategy: The staged transition from individual to group behavior ensures an effective trade-off between exploration and exploitation.

Dynamic Adaptability: Capture rate-driven strategy adjustment allows the algorithm to respond dynamically to the search environment.

Robust Performance: The CFOA exhibits consistent convergence and superior accuracy across a wide range of benchmark problems, making it well-suited for power system optimization.

4. Results and Discussion

4.1. Experiment 1: Power System One Without Nonlinearity

This study evaluates the dynamic performance of the two-area power system presented in Figure 1 under a 0.2 per unit (pu) step load disturbance applied to area 1, with the proposed fuzzy control tuned by the CFOA and PSO (PSO is only for comparative purposes) utilized as an LFC system. Both algorithms were executed over 100 iterations to derive optimal parameters for the fuzzy controller, with the search space constrained to the range [0, 2]. The resultant optimal gain values for the FLC, as determined by the CFOA and PSO, are summarized in Table 3.

Table 3. The optimum values of the Fuzzy FOPID + PI.

Area	Controller	Algorithm	Parameters				
Area one	Fuzzy			**K_1**		**K_2**	
		CFOA		1.9998		1.9992	
		PSO		1.8901		2	
	FOPID		**K_p**	**K_i**	**K_d**	**λ**	**μ**
		CFOA	2	1.998	0.302	1	0.41315
		PSO	1.6463	1.8904	0.5055	1	0.1598
	PI			**K_{p1}**		**K_{I1}**	
		CFOA		2		1.0079	
		PSO		1.5524		0.4903	
Area two	Fuzzy			**K_1**		**K_2**	
		CFOA		0.95497		1.8325	
		PSO		0.1011		2	
	FOPID		**K_p**	**K_i**	**K_d**	**λ**	**μ**
		CFOA	1.9165	1.9996	0.30887	0.0022093	0.99893
		PSO	1.6974	2	1.2743	0.3527	1
	PI			**K_{p1}**		**K_{I1}**	
		CFOA		1.5102		0.10025	
		PSO		0.3622		1.1093	

To assess the efficacy of the proposed FLC, its performance was benchmarked against established control strategies from the literature, including a TLBO-tuned fuzzy PID controller [33] and an LCOA-optimized classical PID controller [8]. Additionally, comparisons were made with conventional PID controllers tuned using the CFOA and PSO under identical test conditions. The corresponding optimal gain parameters for these controllers are detailed in Table 4.

Table 4. Different controllers' optimal gains based on different algorithms.

Controller	**Parameters**							
Fuzzy PID	K_1	K_2	K_3	K_4	K_5	K_6	K_7	K_8
	1.9857	1.9968	1.687	1.9876	1.3469	1.5512	0.809	0.5043
PIDs	K_{P1}	K_{I1}	K_{D1}	K_{P2}	K_{I2}	K_{D2}		
PID-LCOA	0.939	0.7998	0.5636	0.5208	0.4775	0.708		
PID-CFOA	1.8147	2	1.1331	0.090157	1.6888	1.9988		
PID-PSO	1.9987	1.4469	0.79221	1.5327	0.73122	1.2484		

The simulations were conducted in MATLAB/Simulink (2024a), with the CFOA and the PSO algorithm programmed via .m file scripts. The power system models, including controller architectures and disturbance scenarios, were developed within the Simulink environment to ensure reproducibility and alignment with real-time operation practices. As illustrated in Figures 7–9, the proposed Fuzzy FOPID + PI controllers demonstrate superior damping capabilities and rapid response characteristics in both frequency areas and tie-line power deviations.

Specifically, the frequency response in area 1 (Figure 7) shows that the proposed Fuzzy FOPID + PI controller, especially when optimized using the CFOA, yields the lowest undershoot and exhibits fast settling behavior compared to conventional PID-based methods. The controller also ensures smooth convergence with negligible steady-state error. Similarly, in area 2 (Figure 8), the proposed controllers maintain zero overshoot across all schemes while achieving significantly faster recovery and improved transient performance. Notably, the LCOA-PID variant shows the highest peak deviation and the slowest settling time, confirming the enhanced robustness of fuzzy-augmented approaches under complex dynamic conditions.

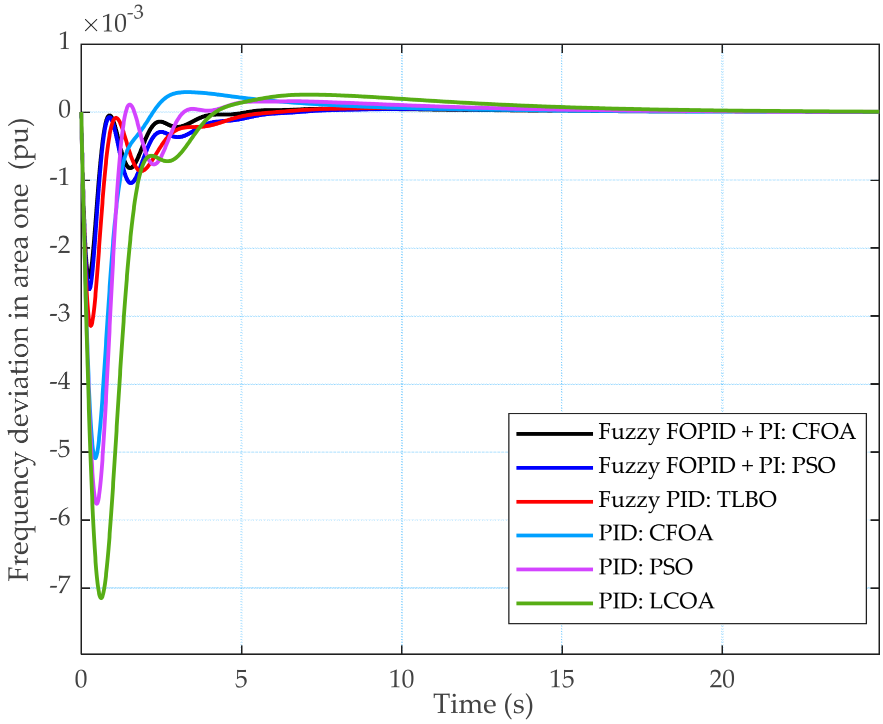

Figure 7. Frequency deviation in area one.

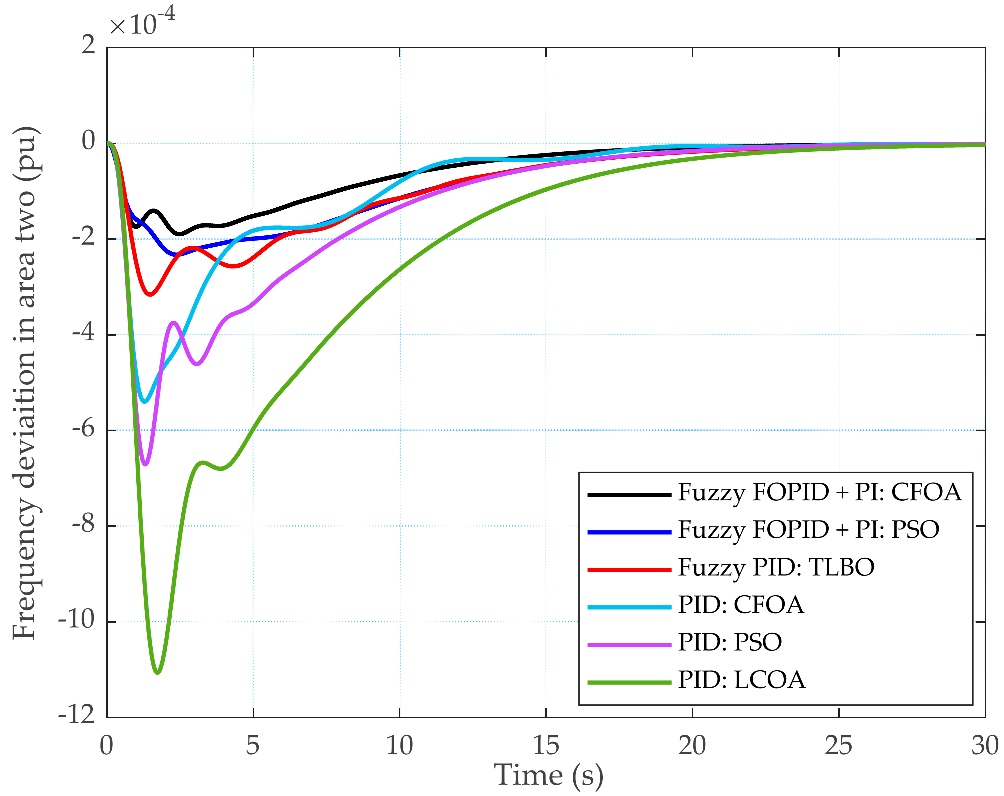

Figure 8. Frequency deviation in area two.

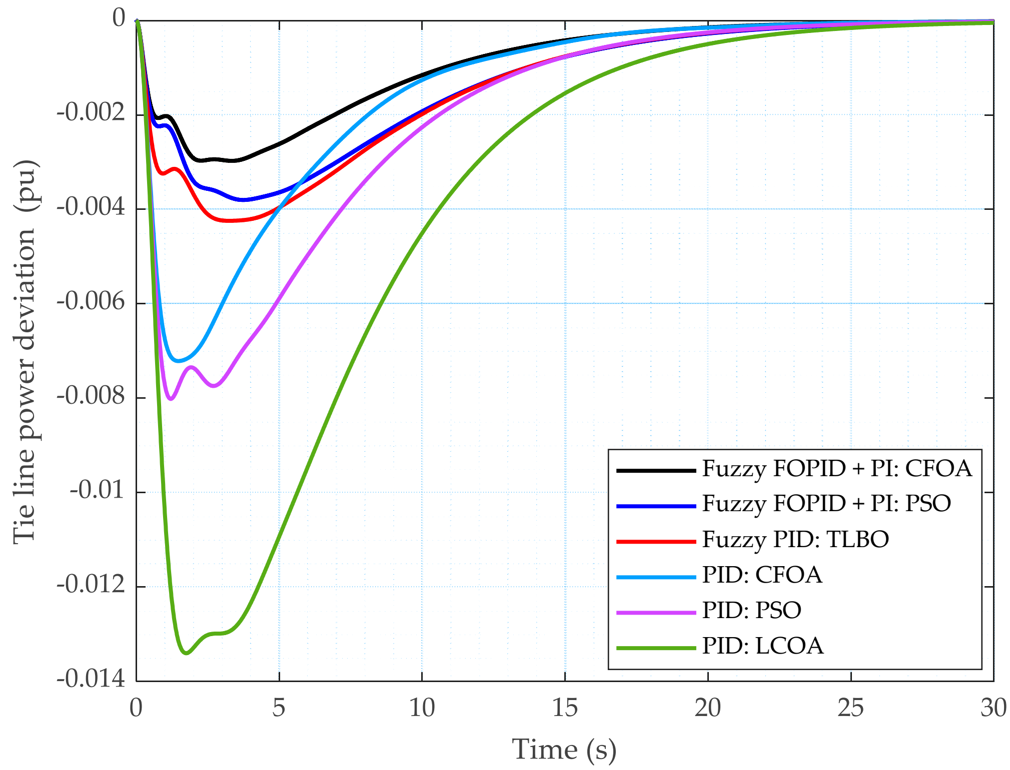

Figure 9. Tie-line power deviation.

Furthermore, the tie-line power deviation profile in Figure 9 underscores the efficacy of the proposed Fuzzy FOPID + PI controllers in minimizing inter-area power oscillations. The zero overshoot in tie-line power for all schemes highlights the overall system stability. However, the CFOA-optimized fuzzy controller achieves the least undershoot and fastest stabilization, aligning with its lowest ITAE value of 0.1992 as presented in Table 5. In contrast, the PID-LCOA controller not only incurs the largest tie-line deviation but also records the highest ITAE value (0.7842), reflecting inefficient control. These observations confirm that the hybrid Fuzzy–CFOA configuration offers a balanced and highly reliable solution for LFC in multi-area power systems, outperforming traditional and soft computing-based PID strategies across all key dynamic performance metrics.

Table 5. Characteristics of the testbed system with different control techniques.

Controller	F1			F2		Tie-Line Power		ITAE
	OS	US	ST	US	ST	US	ST	
Fuzzy–CFOA	4.8696×10^{-5}	-2.425×10^{-3}	3.9471	-1.897×10^{-4}	22.6711	-2.973×10^{-3}	23.0381	0.1992
Fuzzy–PSO	4.5279×10^{-5}	-2.601×10^{-3}	5.4909	-2.325×10^{-4}	24.3901	-3.802×10^{-3}	24.4230	0.3184
Fuzzy–TLBO	5.942×10^{-5}	-3.1422×10^{-3}	4.9936	-3.1594×10^{-4}	23.5188	-0.0042	23.9377	0.3264
PID-CFOA	2.9454×10^{-4}	-5.087×10^{-3}	7.8827	-5.398×10^{-4}	17.9728	-7.214×10^{-3}	19.6328	0.2661
PID-PSO	1.6071×10^{-4}	-5.759×10^{-3}	9.3374	-6.707×10^{-4}	20.2334	-8.015×10^{-5}	21.3580	0.4094
PID-LCOA	2.578×10^{-4}	-7.147×10^{-3}	11.7031	-1.1064×10^{-3}	21.0698	-0.0134	21.9780	0.7842

The bar chart in Figure 10 presents the percentage improvement of fuzzy controllers (Fuzzy–CFOA, Fuzzy–PSO, and Fuzzy–TLBO) compared to the PID-LCOA controller across selected performance metrics: overshoot and undershoot in area 1, undershoot in area 2, tie-line undershoot, and the ITAE. These improvements highlight the superior performance of fuzzy logic controllers, especially Fuzzy–CFOA, in load frequency control applications. As demonstrated in Figure 10, a comparative analysis of the dynamic performance reveals that the fuzzy logic-based controllers demonstrate substantial improvements over the conventional PID-LCOA controller in key performance indices. Specifically, in area 1, the Fuzzy–PSO controller achieves the highest reduction in overshoot, with an improvement of 82.45%, followed closely by Fuzzy–CFOA at 81.1% and Fuzzy–TLBO at 76.95%. Similarly, in terms of undershoot in area 1, Fuzzy–CFOA yields the most significant enhancement (66.0%), indicating a superior damping capability in frequency deviations. For area 2, all fuzzy controllers report marked reductions in undershoot, with Fuzzy–CFOA again outperforming others at 82.7%, followed by Fuzzy–PSO and Fuzzy–TLBO with improvements of 78.9% and 71.45%, respectively. When analyzing the tie-line power undershoot, Fuzzy–CFOA achieves the highest improvement (77.9%), highlighting its effectiveness in inter-area power regulation. Most notably, the Integral of Time-weighted Absolute Error (ITAE)—a critical metric reflecting overall control performance—demonstrates that Fuzzy–CFOA offers the largest improvement (74.6%), indicating a significantly enhanced transient and steady-state response. These findings confirm that fuzzy logic controllers, particularly when optimized using the CFOA, offer a more robust and efficient solution for LFC in interconnected power systems than their PID-based counterparts.

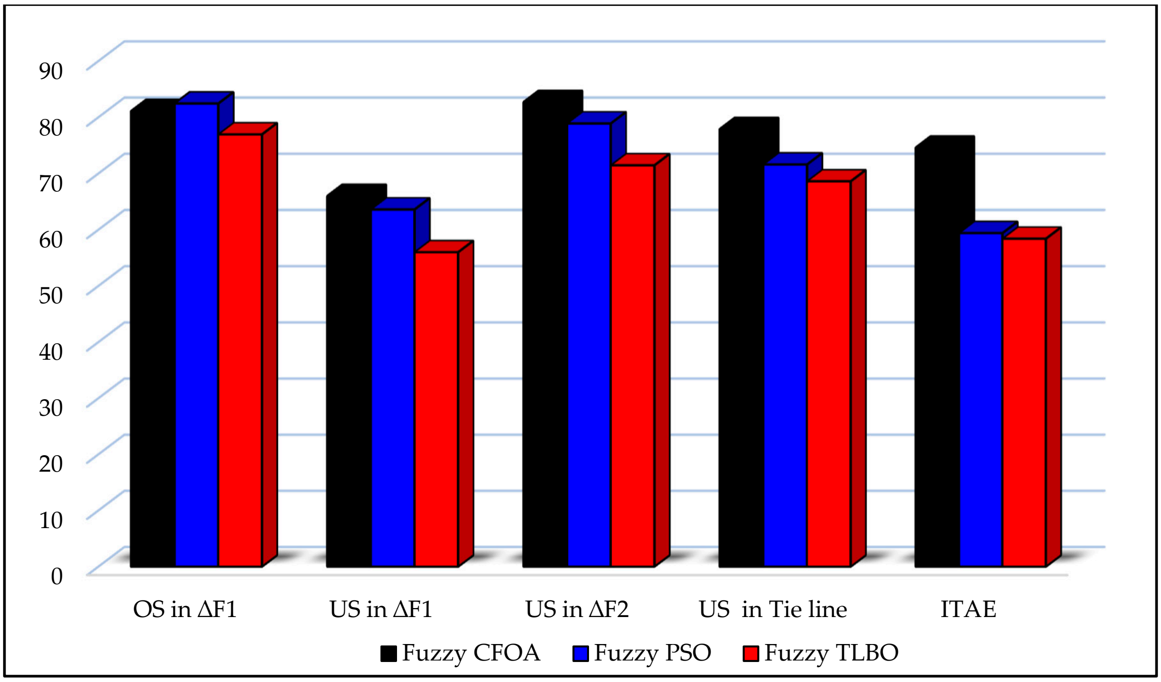

Figure 10. Percentage of improvement in overshoot, undershoot, and ITAE with different controllers.

4.2. Experiment 2: Power System One with GDB

This section investigates the influence of GDB nonlinearities on power system stability by analyzing the GDB component defined in Equation (3) within the framework of the system illustrated in Figure 1. To isolate and elucidate the specific impact of GDB dynamics, the controller parameters optimized under nominal conditions (i.e., linear assumptions, excluding GDB nonlinearity) were retained without retuning. This methodological approach ensured that observed effects were solely attributable to GDB integration, a novel contribution to the literature, as prior studies have not systematically examined this interplay.

Figures 11–13 and Table 6 illustrate the dynamic response of the system when incorporating the GDB element while retaining the fuzzy controller parameters derived under GDB-absent conditions. The results reveal that GDB integration into LFC introduces nonlinear dynamics that substantially degrade system performance characteristics. Specifically, GDB nonlinearities introduce temporal delays in transient responses and induce persistent oscillations following disturbances—phenomena unaccounted for in conventional linear models. The simulation analyses demonstrate pronounced overshoot magnitudes, extended settling durations, and marked deterioration of critical performance metrics, including the ITAE, a pivotal measure of LFC efficacy.

Mechanistically, GBD-induced nonlinearities impede governor response mechanisms to minor frequency deviations, amplifying dynamic instability and, under severe operational stresses, precluding convergence to steady-state equilibrium. These destabilizing effects assume particular significance in multi-area power systems, where frequency stability and coordinated inter-area power exchange are paramount. The findings underscore the necessity of explicitly accounting for GDB nonlinearities during control system synthesis, as overlooking such dynamics risks suboptimal regulatory performance or operational instability under load perturbations.

This investigation highlights a critical gap in traditional LFC design paradigms and provides empirical evidence for the imperative inclusion of GDB dynamics in stability-oriented controller optimization.

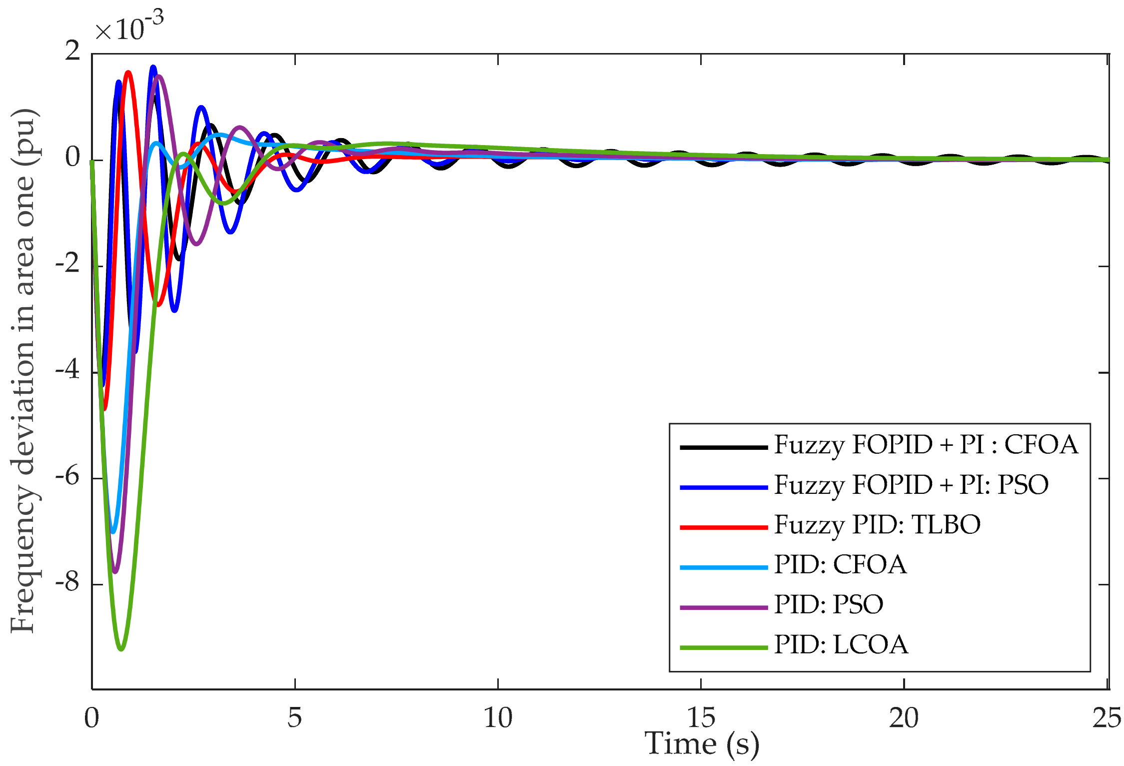

Figure 11. Frequency deviation in area one.

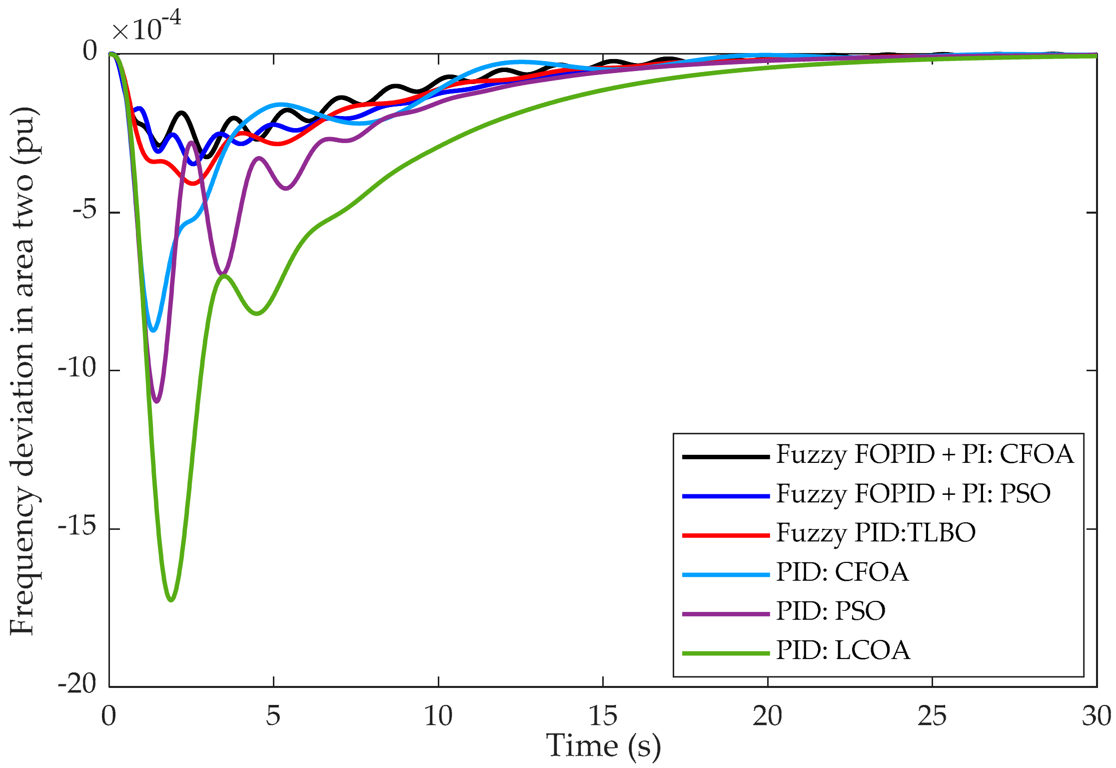

Figure 12. Frequency deviation in area two.

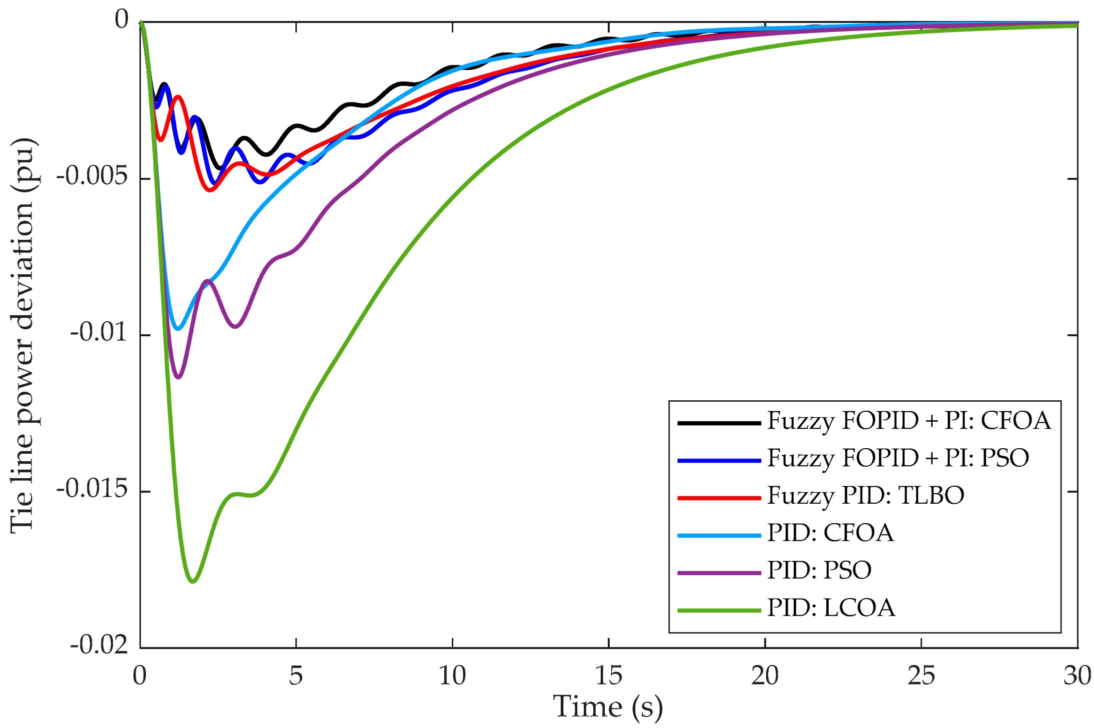

Figure 13. Tie-line power deviation.

Table 6. Characteristics of the testbed system with different control techniques under GDB impact.

Controller	F1			F2			Tie-Line Power		ITAE
	OS	US	ST	OS	US	ST	US	ST	
Fuzzy–CFOA	1.23×10^{-3}	0.0041	21.2599	1.60×10^{-6}	3.2488×10^{-4}	26.2991	0.0047	24.3810	0.3058
Fuzzy–PSO	1.758×10^{-3}	0.0042	13.0079	0	3.4702×10^{-4}	23.3911	0.0051	23.7700	0.383
Fuzzy–TLBO	1.65×10^{-3}	0.0047	4.9043	0	4.0913×10^{-4}	22.6947	0.0054	24.1230	0.3714
PID-CFOA	4.786×10^{-4}	0.0070	7.4226	6.43×10^{-6}	8.7313×10^{-4}	17.7911	0.0098	19.2478	0.3347
PID-PSO	1.576×10^{-3}	0.0078	8.2382	0	0.0011	19.0914	0.0113	21.5307	0.5258
PID-LCOA	3.110×10^{-4}	0.0092	11.1872	0	0.0017	20.3068	0.0179	22.7831	1.016

As evidenced by the experimental results depicted in Figures 11–18 and the comparative analysis summarized in Table 6, the introduction of GDB nonlinearity markedly degraded the dynamic performance of the LFC system, manifesting in suboptimal transient responses and destabilizing oscillations. These findings underscore the imperative of integrating GDB nonlinearity as a critical design parameter in LFC frameworks to ensure operational robustness. To mitigate these adverse effects, the controller parameters of the proposed Fuzzy FOPID + PI hybrid architecture were systematically recalibrated. This optimization process employed the CFOA and PSO—which explicitly incorporated GDB nonlinearity constraints into the tuning procedure. The resultant optimized gain parameters, which demonstrate enhanced stability and performance under nonlinear operating conditions, are comprehensively delineated in Table 7. This methodological refinement highlights the efficacy of advanced optimization techniques in addressing nonlinear dynamics within modern power system control paradigms.

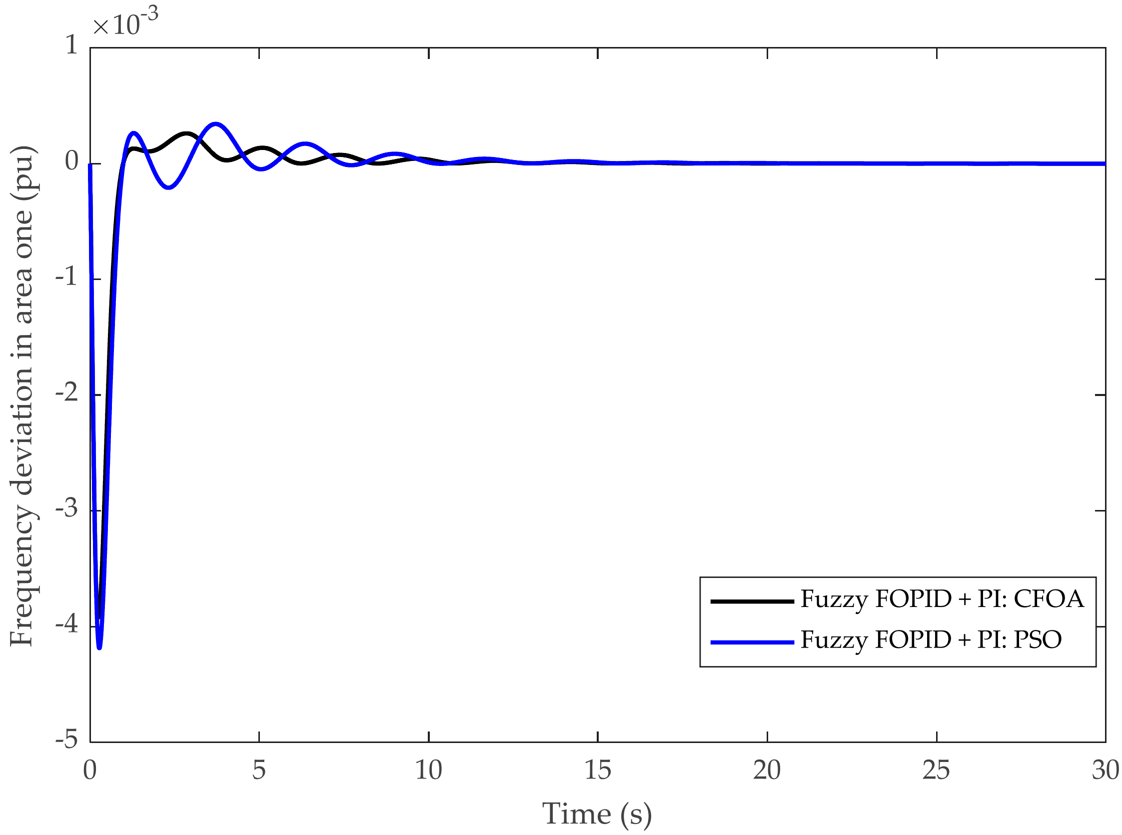

Figure 14. Frequency deviation in area one.

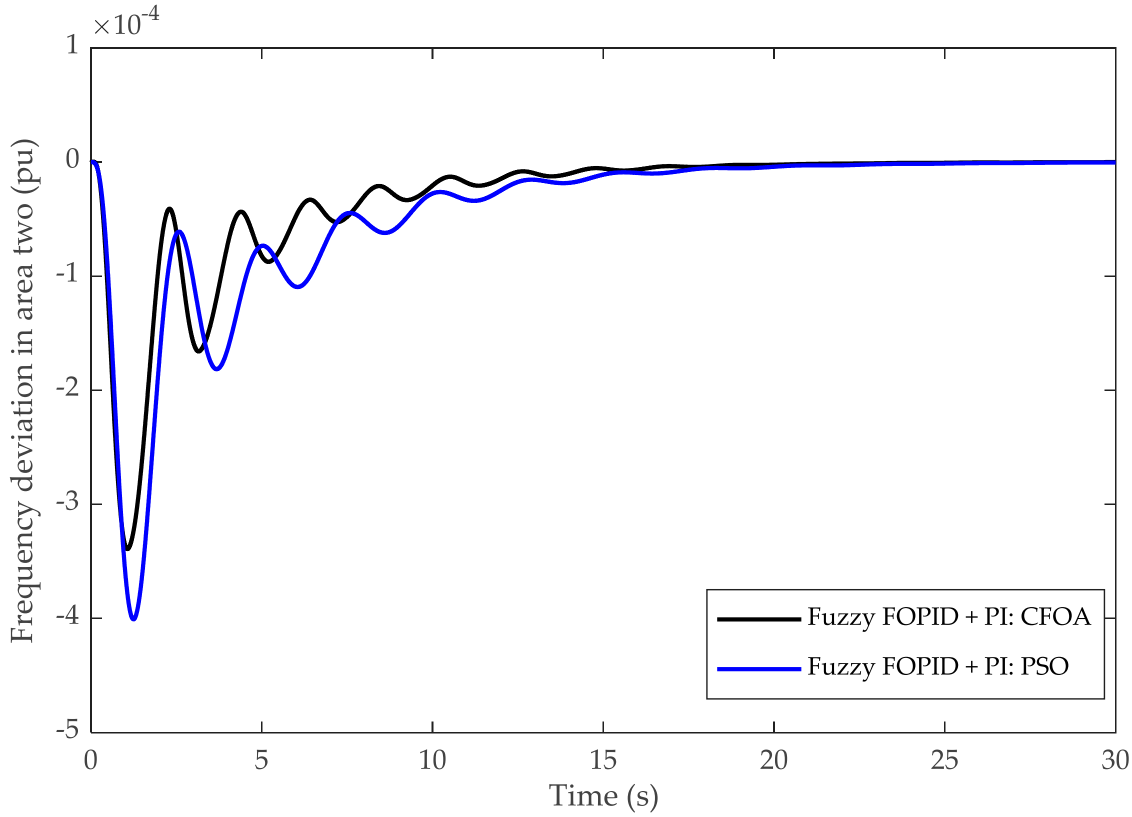

Figure 15. Frequency deviation in area two.

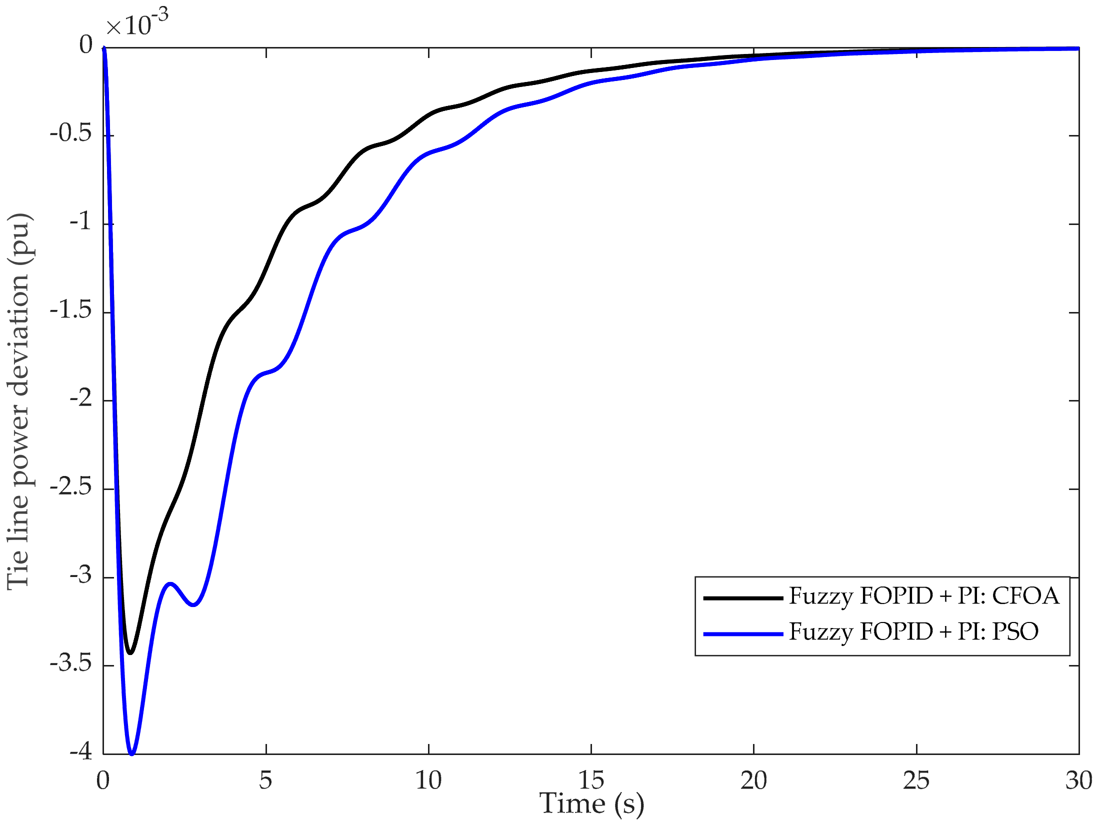

Figure 16. Tie-line power deviation.

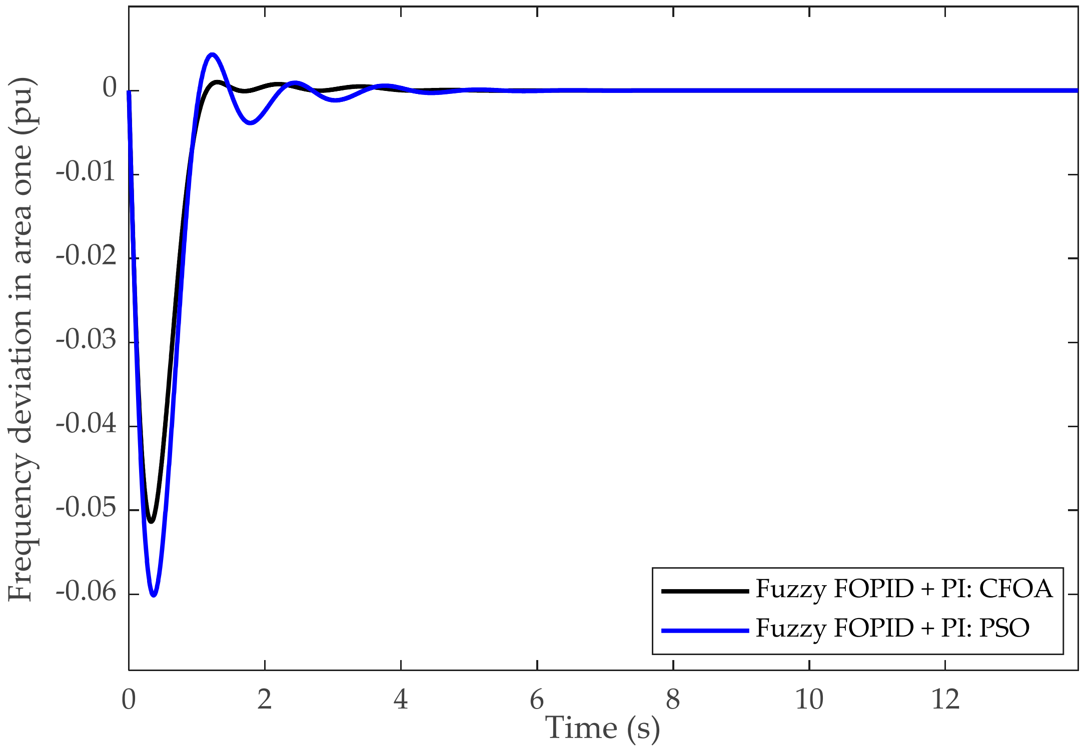

Figure 17. Frequency deviation in area one.

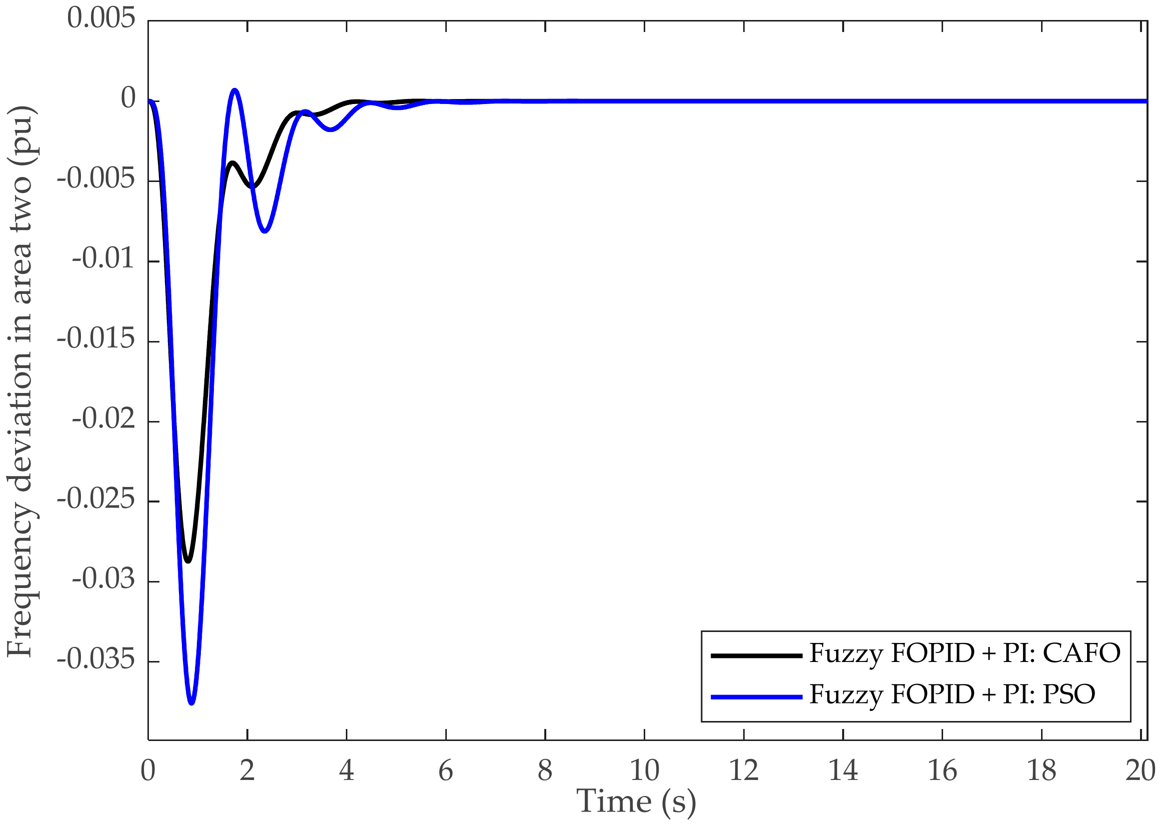

Figure 18. Frequency deviation in area two.

Table 7. The returned optimum values of the Fuzzy FOPID + PI with GDB nonlinearity considered.

Area	Controller	Algorithm	Parameters				
Area one	Fuzzy			K_1		K_2	
		CFOA		1.7932		1.6959	
		PSO		2		0.29701	
	FOPID		K_p	K_i	K_d	λ	μ
		CFOA	0.26328	1.9813	1.4354	0.99354	0.24747
		PSO	1.44	1.9985	1.9999	1	0.76295
	PI			K_{p1}		K_{I1}	
		CFOA		0.60997		1.9956	
		PSO		0.4705		1.9983	
Area two	Fuzzy			K_1		K_2	
		CFOA		1.9474		1.0326	
		PSO		2		1.3405	
	FOPID		K_p	K_i	K_d	λ	μ
		CFOA	1.024	1.8695	1.5135	0.43821	0.86257
		PSO	1.0004	1.2285	1.9851	0.12825	0.70973
	PI			K_{p1}		K_{I1}	
		CFOA		1.9456		1.5507	
		PSO		1.3823		1.0968	

The experimental findings illustrated in Figures 14–16 and quantitatively detailed in Table 8 elucidate the significant enhancements in dynamic response achieved through the proposed control strategies under GDB nonlinearities. Specifically, frequency deviations in both control areas and tie-line power oscillations were markedly attenuated when utilizing fuzzy-based controllers optimized via the CFOA and PSO. Figure 14 highlights the minimized frequency deviation in area 1 under CFOA tuning, exhibiting faster settling and reduced overshoot compared to PSO. Similarly, Figure 15 confirms a smoother frequency response in area 2 with minimized undershoot and quicker stabilization, particularly under the CFOA. These improvements underscore the efficacy of nonlinear-aware optimization in mitigating the destabilizing influence of GDB dynamics, which, as shown in earlier experiments, significantly degraded LFC performance when not explicitly addressed.

Table 8. Characteristics of the testbed system 2 with the proposed LFC fuzzy controller.

Controller	F1			F2			Tie-Line Power		ITAE
	OS	US	ST	OS	US	ST	US	ST	
Fuzzy–CFOA	9.9816×10^{-4}	-5.131×10^{-2}	1.0891	7.18×10^{-6}	-2.872×10^{-2}	3.639	0	-1.01×10^{-2}	3.5664
Fuzzy–PSO	4.275×10^{-3}	-6.012×10^{-2}	2.1084	6.802×10^{-4}	-3.758×10^{-2}	4.090	1.964×10^{-6}	-1.26×10^{-2}	3.9972

Table 8 presents a comprehensive comparison of performance indices—overshoot (OS), undershoot (US), settling time (ST), and the ITAE—for each control configuration. The Fuzzy–CFOA scheme consistently demonstrated superior performance across all metrics. In area 1, this configuration achieved a notably low undershoot (0.0039) and settling time (5.6029 s), while in area 2, the corresponding figures were 0.0034 and 15.9495 s, respectively. Notably, the tie-line power regulation under Fuzzy–CFOA exhibited the fastest settling at 17.8633 s and the lowest ITAE of 0.08467, signifying robust damping characteristics and efficient inter-area coordination. In contrast, the Fuzzy–PSO configuration, while outperforming traditional PID-based designs, yielded slightly higher deviations and prolonged settling periods. These results reinforce the superiority of the CFOA-tuned fuzzy framework in accommodating the nonlinearity introduced by GDB and maintaining system resilience under load perturbations.

The comparative analyses of these figures and metrics offer compelling evidence that incorporating GDB dynamics into the controller tuning phase substantially enhances the robustness of LFC systems. The observed outcomes reflect a paradigm shift from traditional linear design assumptions toward nonlinear-aware optimization strategies. By embedding GDB constraints within the objective functions of the CFOA and PSO, the controllers exhibit heightened adaptability and precision, effectively suppressing frequency oscillations and tie-line power fluctuations. These results not only validate the proposed fuzzy-based hybrid approach as a potent solution for modern power system regulation but also underscore the critical necessity of nonlinear modeling in the design of next-generation LFC architectures.

4.3. Experiment 3: Power System Two Without Nonlinearity

To rigorously assess the effectiveness and generalizability of the proposed controller, it was implemented in an alternative power system configuration distinct from that analyzed in Section 4.1 and 4.2. Specifically, the dynamic behavior of the two-area power system depicted in Figure 2 was evaluated in response to a 0.05 per unit (pu) step load disturbance applied to area 1. In this context, the FLC, optimized using both the CFOA and PSO, was employed to regulate LFC. Each optimization algorithm was executed over 100 iterations to identify the optimal controller parameters, with the search space for each gain constrained within the interval [0, 2]. The resulting optimal gain values for the FLC, as obtained from the CFOA and PSO, are comprehensively presented in Table 9.

Table 9. The optimum values of the Fuzzy FOPID + PI.

Area	Controller	Algorithm	Parameters				
Area one	Fuzzy			K_1		K_2	
		CFOA		0.37564		0.84351	
		PSO		0.3163		0.4863	
	FOPID		K_p	K_i	K_d	λ	μ
		CFOA	1.8576	0.45653	0.36982	0.38209	0.44983
		PSO	0.7276	1.1019	0.9564	0.0896	0.3475
	PI			K_{p1}		K_{I1}	
		CFOA		0.88282		2	
		PSO		0.7935		1.6199	
Area two	Fuzzy			K_1		K_2	
		CFOA		1.3611		1.3818	
		PSO		0.5815		0.8611	
	FOPID		K_p	K_i	K_d	λ	μ
		CFOA	0.9252	1.4084	0.36194	0.64056	0.84815
		PSO	0.5636	1.6106	1.2139	0.6321	0.0762
	PI			K_{p1}		K_{I1}	
		CFOA		1.8829		0.5525	
		PSO		0.4790		1.4447	

The results presented in Figures 17–19, along with the corresponding numerical evaluation in Table 10, demonstrate the dynamic performance of the proposed fuzzy-based controllers in the power system presented in Figure 2 operating under linear conditions. The time-domain responses indicate that the Fuzzy–CFOA configuration consistently outperforms the Fuzzy–PSO across all evaluated metrics. In Figure 17, the frequency deviation in area 1 is effectively minimized by Fuzzy–CFOA, exhibiting significantly faster settling time and lower undershoot compared to the PSO-based alternative. Similarly, Figure 18 illustrates that frequency deviation in area 2 is dampened more efficiently under CFOA tuning, reflecting a more stable and responsive control profile. These enhancements underscore the robustness of the CFOA in determining optimal fuzzy controller gains that enhance transient stability and disturbance rejection.

Table 10. Characteristics of the testbed system with different control techniques considering GDB nonlinearity.

Controller	F1			F2		Tie-Line Power		ITAE
	OS	US	ST	US	ST	US	ST	
Fuzzy–CFOA	2.62×10^{-4}	0.0039	5.6029	3.3919×10^{-4}	15.9495	0.0034	17.8633	0.08467
Fuzzy–PSO	3.435×10^{-4}	0.0042	9.1031	4.0081×10^{-4}	17.1281	0.0040	19.1061	0.1267

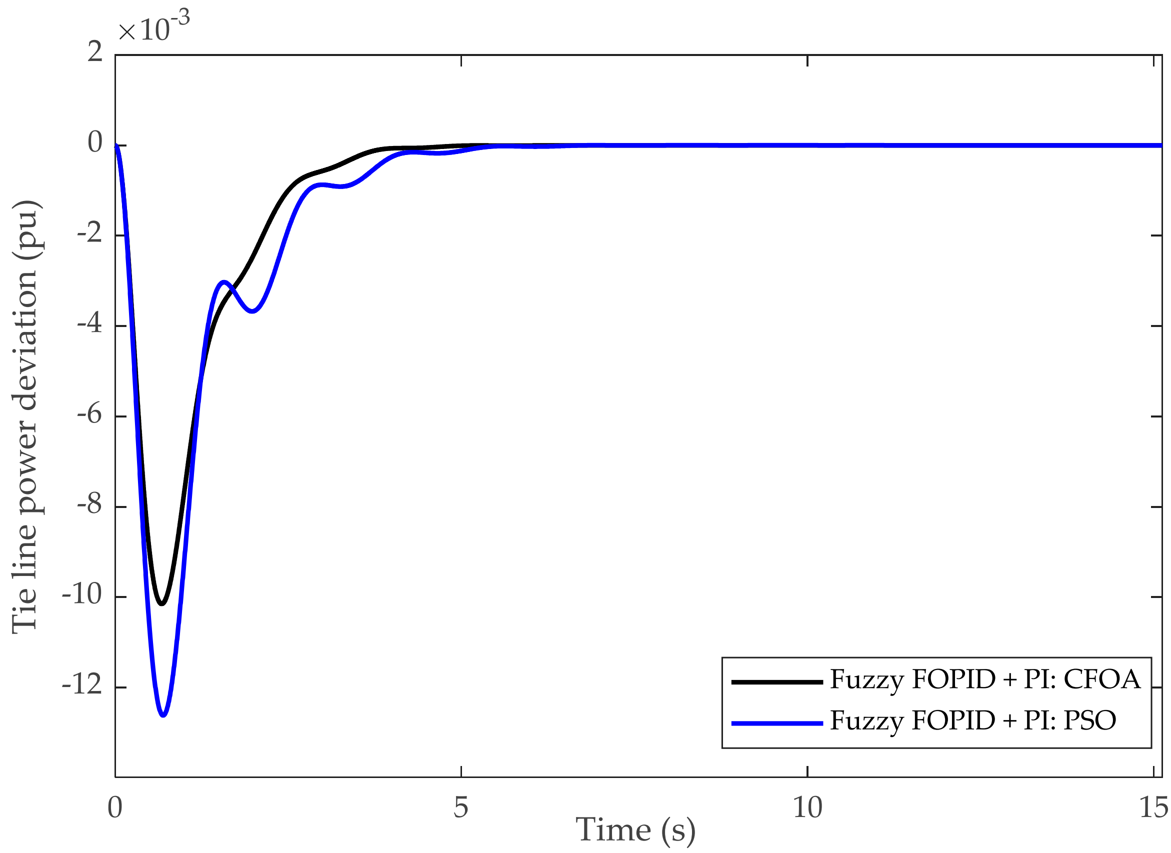

Figure 19. Tie-line power deviation.

Figure 19 further substantiates the superior performance of the Fuzzy–CFOA configuration in managing tie-line power deviations. Under a 0.05 pu step load disturbance, the Fuzzy–CFOA controller rapidly stabilizes inter-area power oscillations, achieving a lower magnitude of deviation and a shorter settling period relative to Fuzzy–PSO. These characteristics are critical in multi-area systems where tie-line power regulation directly impacts overall system coordination and frequency synchronization. The comparative visual trends across the three figures confirm the advantage of the CFOA in maintaining system equilibrium during transients, particularly when operating under ideal linear conditions devoid of nonlinear disturbances, such as governor dead band effects.

Table 10 quantitatively reinforces the qualitative trends observed in the figures. The Fuzzy–CFOA controller achieves the lowest Integral of Time-weighted Absolute Error (ITAE) value of 0.08467, indicating superior control effort and transient accuracy. It also delivers the shortest settling times across all performance outputs, with values of 5.6029 s for area 1 frequency, 15.9495 s for area 2 frequency, and 17.8633 s for tie-line power. These results suggest that the CFOA not only ensures faster convergence but also enhances stability margins and system reliability. Although Fuzzy–PSO demonstrates competent performance, its relatively higher overshoot, undershoot, and ITAE values indicate a less precise tuning capability compared to the CFOA. Overall, the findings validate the proposed fuzzy–CFOA controller as a highly effective solution for linear LFC environments.

4.4. Experiment 4: Power System Two with GRCs

This section investigates the influence of generation rate constraints (GRCs) on power system stability by integrating the GRC mechanism, as depicted in Figure 3, into the two-area power system architecture presented in Figure 2. To explicitly isolate the dynamic impact of GRCs, the fuzzy controller parameters—previously optimized under nominal, linear operating assumptions without GRCs—were preserved without further retuning.

This methodological approach enabled a clear and unbiased evaluation of GRC-induced effects, offering a novel contribution to the literature, as prior studies have seldom addressed the interaction between GRC dynamics and pre-optimized fuzzy control structures. Figures 20–22 illustrate the system's dynamic responses following the incorporation of GRCs, while retaining the controller gains optimized for the linear operating conditions outlined in Table 9.

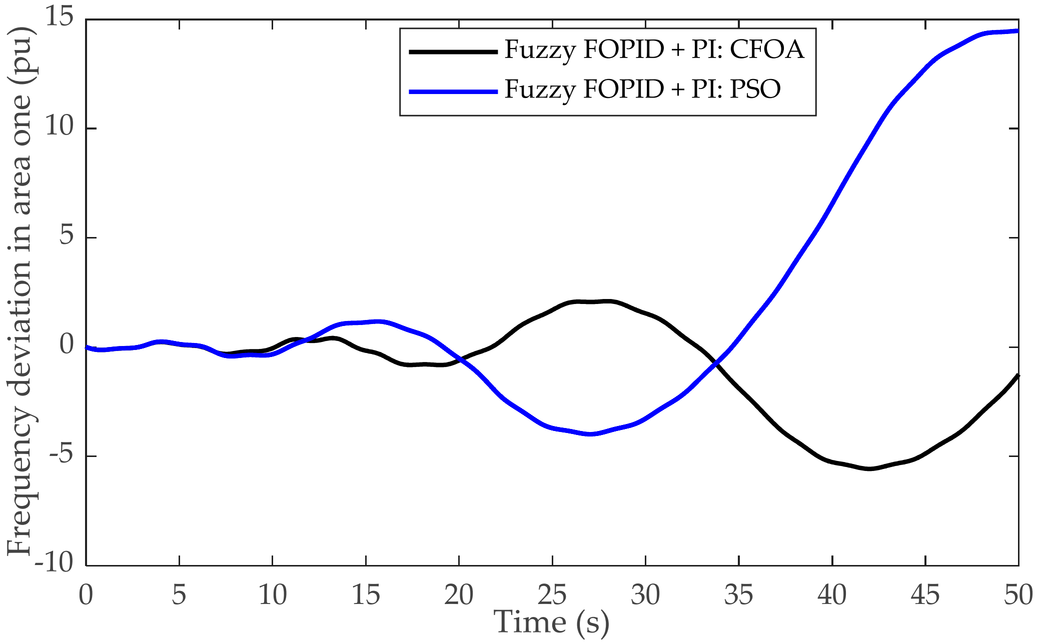

Figure 20. Frequency deviation in area one.

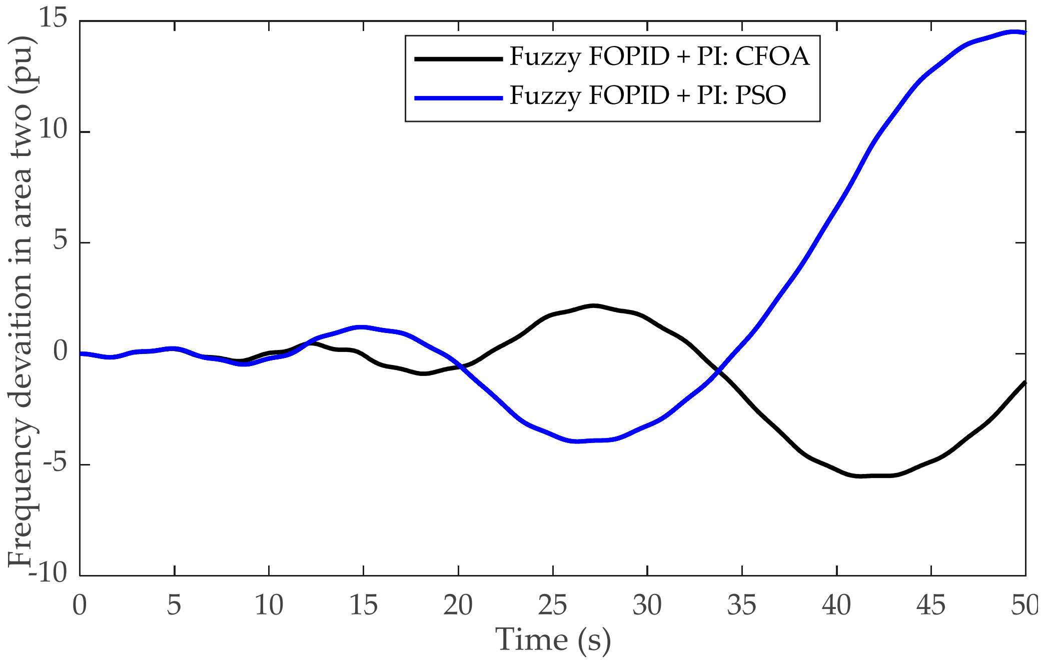

Figure 21. Frequency deviation in area two.

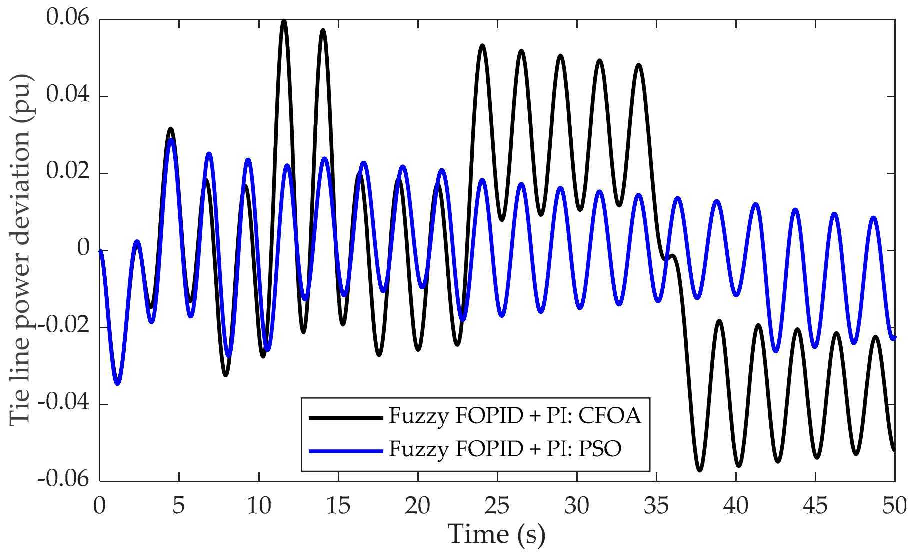

Figure 22. Tie-line power deviation.

The experimental results presented in Figures 20–22 demonstrate that the incorporation of GRC nonlinearity significantly compromises the dynamic performance of the LFC system, ultimately driving it toward instability. These findings highlight the necessity of accounting for GRC nonlinearity as a fundamental design consideration in LFC systems to ensure operational reliability. The simulation findings also suggest that LFC strategies developed without considering GRC effects may fail to perform adequately in real-world implementations. To address these destabilizing effects, the controller parameters of the proposed Fuzzy FOPID + PI hybrid control structure were meticulously reoptimized. This tuning process used the CFOA and the PSO algorithm, with GRC nonlinearity constraints explicitly integrated into the testbed system. The optimized gain parameters, detailed in Table 11, exhibit improved stability and control performance under nonlinear operating conditions, as shown in Figures 23–25. This methodological enhancement underscores the effectiveness of advanced optimization techniques in managing nonlinear dynamics within contemporary power system control architectures.

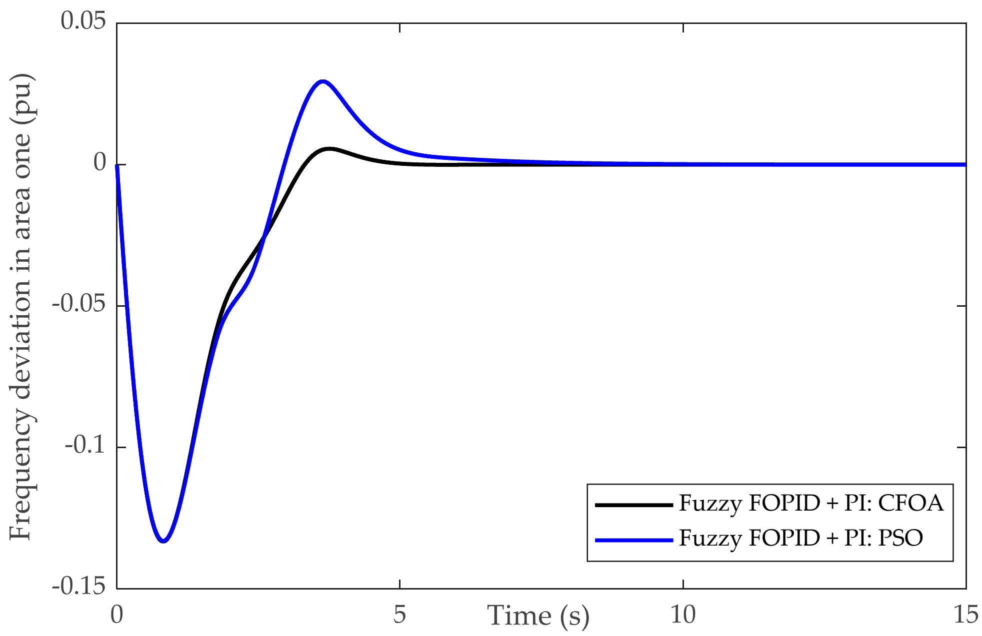

Figure 23. Frequency deviation in area one.

Table 11. The optimum values of the Fuzzy FOPID + PI.

Area	Controller	Algorithm	Parameters				
Area one	Fuzzy			**K_1**		**K_2**	
		CFOA		1.998677		0.1283334	
		PSO		1.5778		1.2389	
	FOPID		**K_p**	**K_i**	**K_d**	**λ**	**μ**
		CFOA	1.7994	0.32883	1.1732	0.40964	0.55149
		PSO	1.3747	0.25468	1.9624	0.41568	0.35223
	PI			**K_{p1}**		**K_{I1}**	
		CFOA		0.51443		0.37854	
		PSO		0.57469		0.34591	
Area two	Fuzzy			**K_1**		**K_2**	
		CFOA		1.5667		1.712	
		PSO		1.2814		1.4995	
	FOPID		**K_p**	**K_i**	**K_d**	**λ**	**μ**
		CFOA	1.9536	0.56448	1.5143	0.014586	0.98738
		PSO	1.7496	0.50135	1.3866	0.63994	0.7015
	PI			**K_{p1}**		**K_{I1}**	
		CFOA		0.76396		0.0064206	
		PSO		0.92753		1.2186	

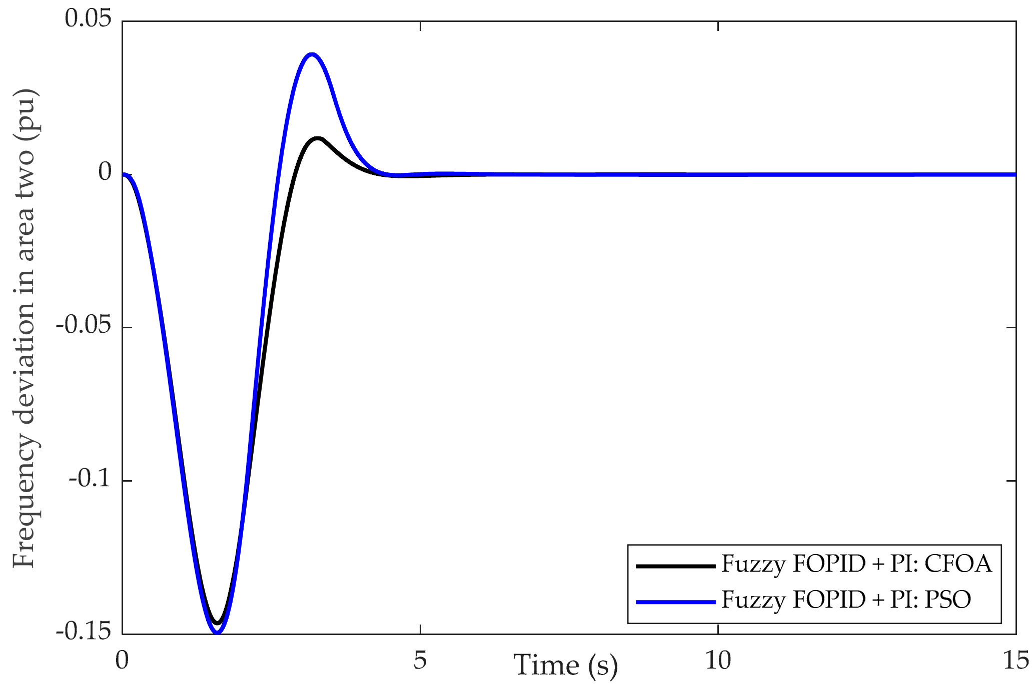

Figure 24. Frequency deviation in area two.

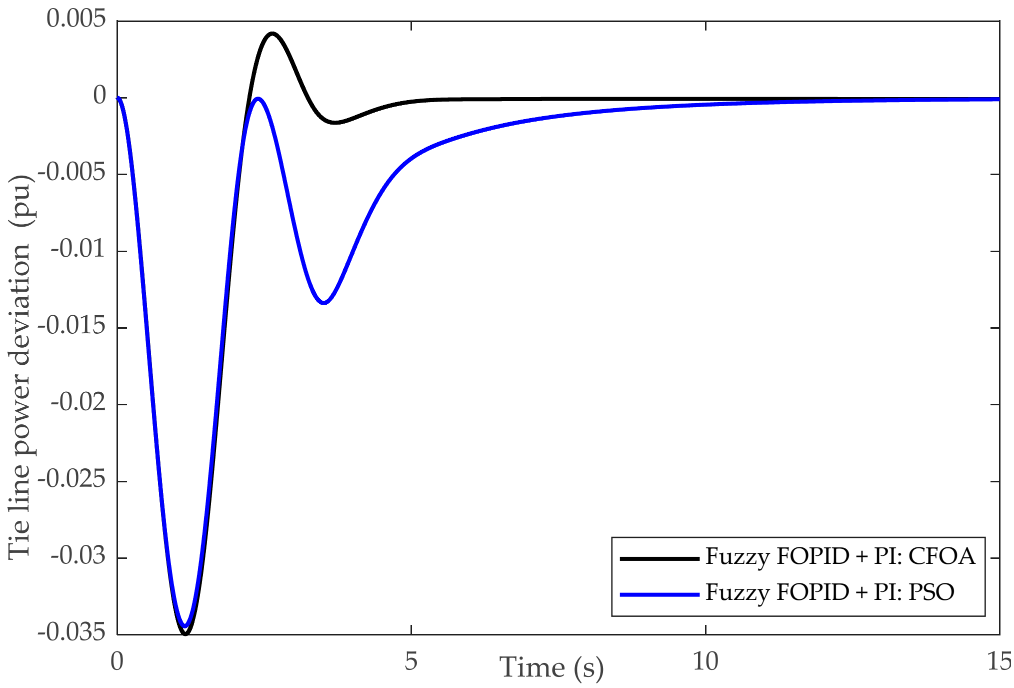

Figure 25. Tie-line power deviation.

Figures 23–25 illustrate the dynamic response of a two-area power system equipped with fuzzy-based controllers under the influence of GRCs, with the controller parameters optimized using both the CFOA and the PSO algorithm. Figure 23, representing the frequency deviation in area 1, reveals that the Fuzzy–CFOA controller achieves a faster settling time and lower overshoot/undershoot relative to the Fuzzy–PSO counterpart. Similarly, Figure 24, depicting the frequency response in area 2, affirms this trend; the CFOA-optimized controller exhibits superior damping characteristics and a more stable trajectory in managing frequency fluctuations post-disturbance. In both cases, the CFOA-based design ensures improved transient performance, thereby emphasizing the efficacy of the proposed controller even when considering the impact of the GRC element.

The tie-line power deviations shown in Figure 25 further substantiate the robustness of the CFOA-optimized controller under nonlinear conditions introduced by GRCs. While both algorithms manage to stabilize the inter-area oscillations, the Fuzzy–CFOA configuration maintains a lower magnitude of oscillatory behavior and achieves equilibrium significantly faster than its PSO-tuned counterpart. This enhanced performance in tie-line regulation is critical in maintaining coherent operation across interconnected control areas. The comparative performance across Figures 23–25 highlights the necessity of considering nonlinear elements, like GRCs, when designing an LFC system to avoid degradation in system stability and responsiveness.

Table 12 provides a comprehensive summary of the optimized gain values for the hybrid Fuzzy FOPID + PI controller under GRCs. It details the parameter sets derived via the CFOA and PSO for both control areas, capturing the diverse controller structures and fractional-order terms employed. Notably, the CFOA yields higher accuracy with improved ITAE values (0.7026) compared to PSO (1.036), alongside better performance in terms of overshoot, undershoot, and settling time metrics across all outputs—area 1 and area 2 frequencies and tie-line power. These quantitative insights corroborate the qualitative analysis of Figures 23–25, affirming that the CFOA offers a more reliable and effective approach for handling nonlinear dynamics in modern LFC frameworks.

Table 12. Characteristics of the testbed system with different control techniques considering GRC nonlinearity.

Controller	F1			F2			Tie-Line			ITAE
	OS	US	ST	OS	US	ST	OS	US	ST	
Fuzzy–CFOA	5.64×10^{-3}	−0.133	4.3160	0.01185	0.1464	3.9078	4.18×10^{-3}	0.0350	4.3962	0.7026
Fuzzy–PSO	0.029466	0.1331	5.6289	0.0392	0.1496	4.1170	0	0.0344	8.5264	1.036

4.5. Experiment 5: Robustness Analysis Against Parametric Uncertainty

The parameters within the system—such as the damping coefficient, speed regulator, system inertia coefficient, and turbine governor time constant—are prone to continuous fluctuations, which can substantially impair the performance of closed-loop control systems. Despite their critical influence, research on this issue in the context of LFC remains relatively limited. For instance, an increase in total system inertia tends to decelerate the system response, whereas a higher damping ratio reduces frequency deviation. Conversely, an increase in the governor time constant exacerbates frequency deviation.

In this section, the robustness of the proposed Fuzzy FOPID + PI controller, optimized using the CFOA, is rigorously evaluated under significant parametric uncertainties within a two-area interconnected power system that includes GDB nonlinearity. Eight distinct test cases (Table 13) are formulated by varying critical system parameters—such as the inertia constant (H), the damping coefficient (D), the speed regulation constant (R), the turbine time constant (Tt), the governor time constant (Tg), and frequency bias (B)—by ±35% from their nominal values. Importantly, the optimal gains of the proposed Fuzzy FOPID + PI controller (presented in Table 3) based on the CFOA, derived under normal operating conditions, remain fixed and are not retuned despite variations in system parameters.

Table 13. Different investigated scenarios of system parametric uncertainties.

Case No.	Parameter	Area 1	Area 2	Variation Range	Area 1	Area 2
Case 1	H	5	4	+35%	6.75	5.4
Case 2	D	0.6	0.9	−35%	0.39	0.585
Case 3	R	0.05	0.0625	+35%	0.0675	0.0844
Case 4	Tt	0.5	0.6	−35%	0.325	0.39
Case 5	B	20.6	16.9	+35%	27.81	22.815
Case 6	D	0.6	0.9	+35%	0.81	1.215
Case 7	Tg	0.2	0.3	−35%	0.13	0.195
Case 8	R	0.05	0.0625	−35%	0.0325	0.0406

Figures 26–28 illustrate the frequency deviations in area one and area two, as well as the tie-line power deviations across all eight cases. These graphical results collectively affirm that the controller maintains stable and bounded responses despite significant parameter perturbations. Table 14 quantitatively summarizes the system's dynamic responses under each test case, reporting metrics such as overshoot (OS), undershoot (US), settling time (ST), and the ITAE for frequency deviations in both areas and tie-line power.

The analysis reveals that the proposed controller demonstrates commendable robustness. In Case 1, where system inertia is increased by 35%, the controller manages to suppress overshoots effectively, albeit with a slightly prolonged settling time in both areas. Cases 2 and 6, which examine variations in damping, exhibit the fastest settling times (5.6320 s and 5.5843 s in area 1, respectively), confirming that higher damping enhances system stability. Conversely, Case 5, involving a +35% increase in the frequency bias (B), results in the highest ITAE (0.2264), indicating that such changes impose a greater burden on the control system. Despite this, frequency deviations remain within acceptable limits, and no instability is observed.

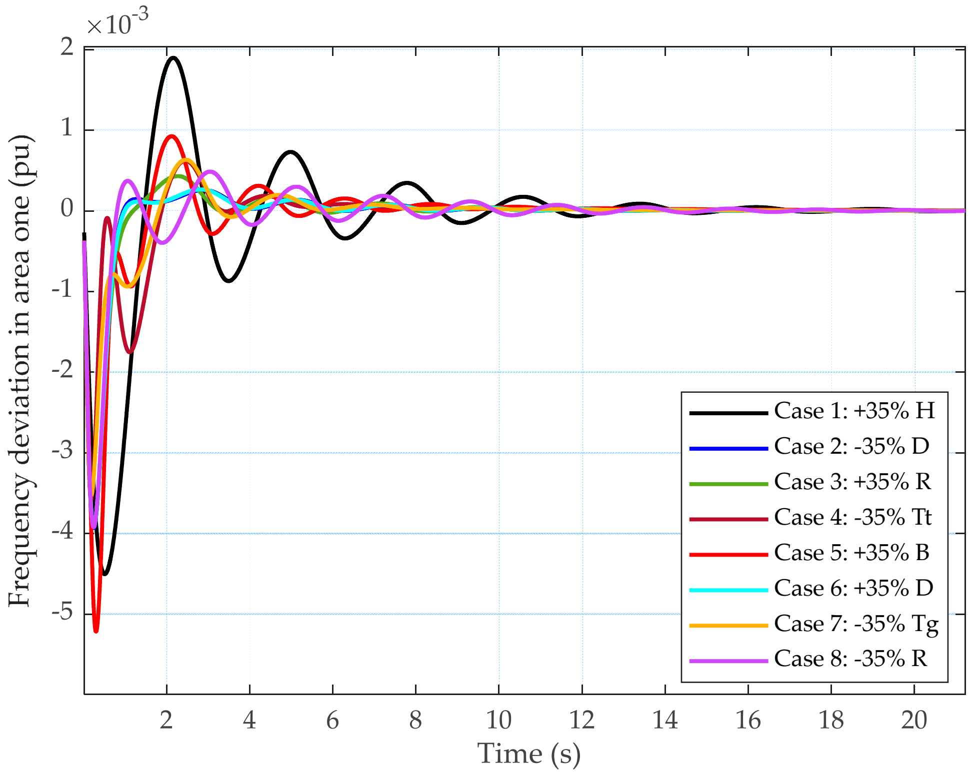

Figure 26. Frequency deviation in area one.

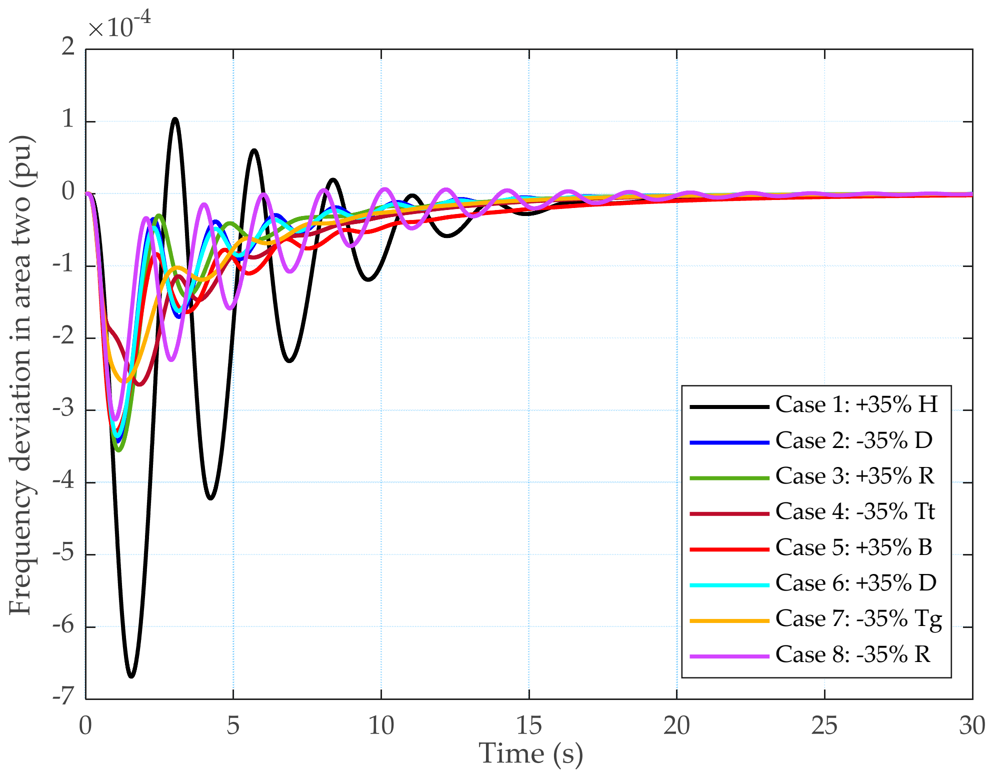

Figure 27. Frequency deviation in area two.

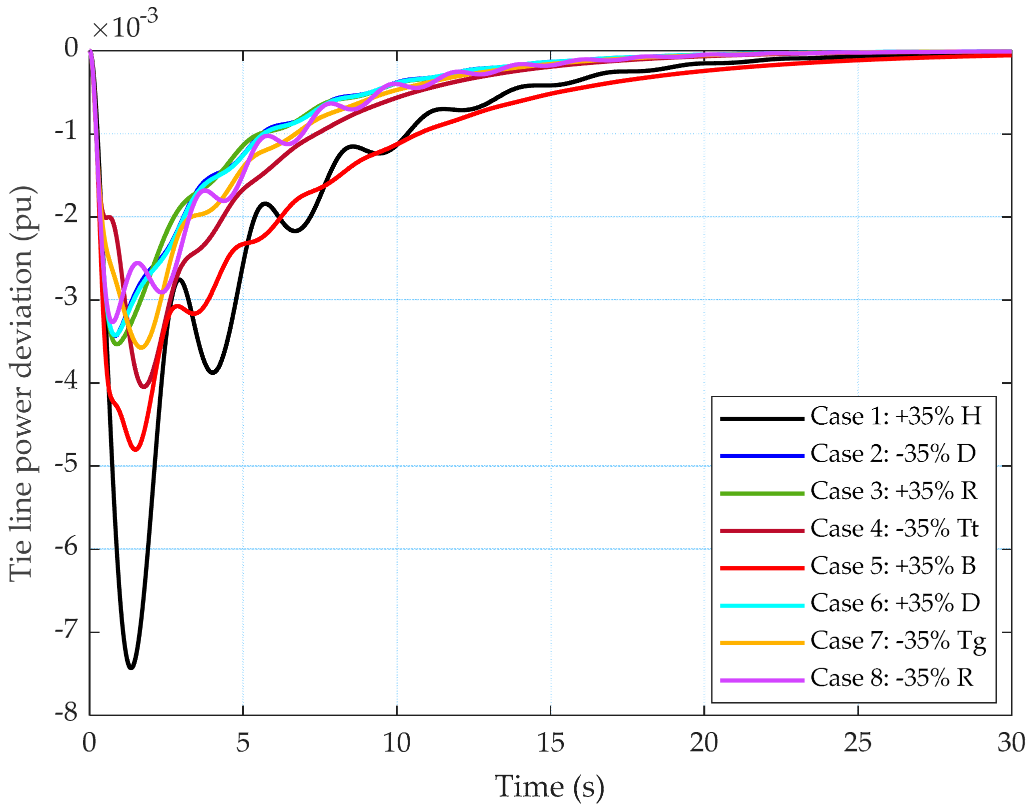

Figure 28. Tie-line power deviation.

Table 14. Dynamic response of the system under different parametric uncertainty cases with the fuzzy controller.

Case No.	F1			F2			Tie-Line		ITAE
	OS	US	ST	OS	US	ST	US	ST	
Case 1	1.898×10^{-3}	-4.50×10^{-3}	11.0830	1.03×10^{-4}	-6.68×10^{-4}	16.0275	-7.431×10^{-3}	19.2488	0.2225
Case 2	2.591×10^{-4}	-3.93×10^{-3}	5.6320	0	-3.43×10^{-4}	16.0203	-3.432×10^{-3}	17.8825	0.08452
Case 3	4.317×10^{-4}	-3.91×10^{-3}	7.4107	0	-3.55×10^{-4}	14.6044	-3.532×10^{-3}	17.9442	0.08631
Case 4	6.218×10^{-4}	-3.57×10^{-3}	6.6621	0	-2.64×10^{-4}	17.8677	-4.045×10^{-3}	18.5645	0.1177
Case 5	9.253×10^{-4}	-5.21×10^{-3}	6.6483	0	-3.29×10^{-4}	20.7906	-4.801×10^{-3}	23.1913	0.2264
Case 6	2.663×10^{-4}	-3.90×10^{-3}	5.5843	0	-3.35×10^{-4}	15.9009	-3.242×10^{-3}	17.8491	0.08493
Case 7	6.338×10^{-4}	-3.51×10^{-3}	7.2140	0	-2.60×10^{-4}	17.1571	-3.573×10^{-3}	18.2752	0.09975
Case 8	4.86×10^{-4}	-3.91×10^{-3}	9.6209	6.5×10^{-6}	-3.12×10^{-4}	19.6390	-3.265×10^{-3}	19.1245	0.1007

In summary, the proposed Fuzzy FOPID + PI controller maintains high performance and resilience under a wide spectrum of parametric uncertainties. These results underscore its suitability for practical deployment in complex and variable LFC environments, especially where retuning is impractical or costly. Nonetheless, further exploration incorporating additional nonlinearities and operational constraints would enrich the comprehensiveness of the robustness assessment.

5. Conclusions and Future Work

This study has introduced a robust and adaptive load frequency control (LFC) framework incorporating a hybrid Fuzzy FOPID enhanced by a PI controller optimized using the Catch Fish Optimization Algorithm (CFOA). The proposed control architecture demonstrates superior performance in multi-area power systems by effectively integrating fractional-order dynamics with fuzzy logic inference and classical PI compensation. Through comprehensive testing on two benchmark systems—under both linear and nonlinear operating conditions—the controller consistently exhibited excellent damping characteristics, rapid frequency stabilization, and minimal tie-line power deviations. Importantly, the inclusion and systematic evaluation of critical nonlinearities such as governor dead band (GDB) and generation rate constraints (GRCs) validated the controller's resilience under practical operational constraints. Comparative analyses further affirmed that the CFOA outperformed conventional algorithms like PSO. Moreover, the proposed Fuzzy–CFOA controller achieved up to an 82.7% reduction in frequency undershoot, a 77.9% improvement in tie-line power regulation, and a 74.6% reduction in ITAE compared to traditional PID-based schemes, confirming its superior dynamic and steady-state performance. While this study focused on the nonlinear impacts of governor dead band (GDB) and generation rate constraints (GRCs), other nonlinearities, such as actuator saturation, dead-time, backlash, and time delays, are also known to affect control stability and should be considered in future investigations. Overall, the results underscore the controller's effectiveness in ensuring dynamic stability, making it a promising candidate for deployment in modern, nonlinear power grids. It is also evident that new proposals for LFC systems should always take into account the nonlinear impact within the system when designing new controllers.

Building on the promising results of this investigation, future research should focus on the following trajectories:

1. Hardware-in-the-Loop (HIL) Validation: Integrating the proposed control scheme into real-time simulation platforms or microgrid testbeds to validate performance under physical constraints and communication delays.
2. Extension to Multi-Source Renewable Systems: Expanding the controller application to multi-area systems comprising wind, solar, and battery storage units to test robustness under intermittent generation.
3. Cyber–Physical Security and Communication Delays: Incorporating cyber-attack scenarios and latency in data transmission to assess controller reliability in smart grid infrastructures.
4. Investigation of Additional Nonlinearities**:** Incorporating other practical nonlinear elements, including actuator saturation, backlash, and dead time, to further evaluate the robustness of the proposed controller in more realistic power system environments.

Author Contributions: Conceptualization, M.S. and S.A.; methodology, M.S. and S.A.; software, M.S. and S.A.; validation, M.S., S.A. and F.A.; formal analysis, M.P.; investigation, M.S. and S.A.; resources, M.P.; data curation, F.A.; writing—original draft preparation, M.S., F.A., M.P. and S.A.; writing—review and editing, M.S., F.A., M.P. and S.A.; visualization, M.S., F.A., M.P. and S.A.; supervision, F.A.; project administration, M.P.; funding acquisition, S.A. All authors have read and agreed to the published version of the manuscript.

Funding: This research received no external funding.

Data Availability Statement: No data was used to produce this manuscript. The conducted codes and simulations are available upon a reasonable request from the corresponding author.

Acknowledgments: The authors would like to thank Cardiff University, School of Engineering, for paying the APC required to publish this manuscript.

Conflicts of Interest: The authors declare no conflicts of interest.

Abbreviations

The following abbreviations are used in this manuscript:

LFC	load frequency control
FOPID	fractional-order proportional–integral–derivative
PI	proportional and integral
FLC	fuzzy logic controller
CFOA	catch fish optimization algorithm
ITAE	integral of time-weighted absolute error
GDB	governor dead band
GRC	generation rate constraint
PSO	particle swarm optimization
GA	genetic algorithm
ITEA	integral of time multiplied error in area
ACE	area control error
MF	membership function
NB	negative big
NS	negative small
Z	zero
PS	positive small
PB	positive big
SLP	step load perturbation
DG	distributed generation
BES	battery energy storage
SMES	superconducting magnetic energy storage
RES	renewable energy sources
AVR	automatic voltage regulator
TLBO	teaching–learning-based optimization
PIDF	proportional, integral, derivative with filter
FOPI	fractional-order proportional–integral
FOPD	fractional-order proportional—-derivative

Appendix A

The nominal parameters adopted for the two-area power system model 1 are as follows:

F = 60 Hz; R_1 = 0.05 MW/Hz; R_2 = 0.0625 MW/Hz; B_1 = 20.6 Hz/MW; B_2 = 16.9 Hz/MW; SLP = 0.2 pu; T_{g1} = 0.2 s; T_{g2} = 0.3 s; T_{t1} = 0.5 s; T_{t2} = 0.6 s; H_1 = 5; H_2 = 4; D_1 = 0.6; D_2 = 0.9; T = 2.

Appendix B

The nominal parameters adopted for the two-area power system model 2 are as follows:

F = 60 Hz; $R_1 = R_2$ = 0.05 MW/Hz; $B_1 = B_2$ = 0.425 Hz/MW; SLP = 0.05 pu; $T_{g1} = T_{g2}$ = 0.08 s; $T_{t1} = T_{t2}$ = 0.3 s; $T_{P1} = T_{P2}$ = 20 s; $K_{P1} = K_{P2}$ = 120; $a_{12} = -1$; T_{12} = 0.545.

References

1. Gulzar, M.M.; Sibtain, D.; Alqahtani, M.; Alismail, F.; Khalid, M. Load frequency control progress: A comprehensive review on recent development and challenges of modern power systems. *Energy Strat. Rev.* **2024**, *57*, 101604. [CrossRef]
2. Almutairi, S.Z.; Moustafa, G.; Hakmi, S.H.; Shaheen, A.M. Bonobo Optimizer Inspired PI-(1+DD) Controller for Robust Load Frequency Management in Renewable Wind Energy Systems. *Int. J. Energy Res.* **2025**, *2025*, 6874402. [CrossRef]
3. Tuan, D.H.; Nguyen Ngoc Thanh, V.; Nguyen Chi, D.; Pham, V.H. Improving Frequency Control of Multi-Area Interconnected Hydro-Thermal Power System Using PSO Algorithm. *Appl. Sci.* **2025**, *15*, 2898. [CrossRef]

4. Shankar, R.; Pradhan, S.R.; Chatterjee, K.; Mandal, R. A comprehensive state of the art literature survey on LFC mechanism for power system. *Renew. Sustain. Energy Rev.* **2017**, *76*, 1185–1207. [CrossRef]
5. Shouran, M.; Anayi, F.; Packianather, M. A State-of-the-Art Review on LFC Strategies in Conventional and Modern Power Systems. In Proceedings of the 2021 International Conference on Advance Computing and Innovative Technologies in Engineering (ICACITE), Greater Noida, India, 4–5 March 2021; pp. 268–277. [CrossRef]
6. AboRas, K.M.; Sedik, A.M.A.; Hammad, M.R. Hybrid dual-area power grid frequency fluctuation effective control utilizing a maiden combination of MOA-based 1 + PIID and $PD^{\mu}F^{\lambda}$ controllers. *Sci. Prog.* **2025**, *108*, 00368504251330521. [CrossRef]
7. Kozák, Š. State-of-the-art in control engineering. *J. Electr. Syst. Inf. Technol.* **2014**, *1*, 1–9. [CrossRef]
8. Ekinci, S.; Izci, D.; Turkeri, C.; Smerat, A.; Ezugwu, A.E.; Abualigah, L. Frequency regulation of two-area thermal and photovoltaic power system via flood algorithm. *Results Control Optim.* **2025**, *18*, 100539. [CrossRef]
9. Abd-Elazim, S.M.; Ali, E.S. Load frequency controller design of a two-area system composing of PV grid and thermal generator via firefly algorithm. *Neural Comput. Appl.* **2016**, *30*, 607–616. [CrossRef]
10. Pearce, J.M. Load Frequency Control Assessment of a PSO-PID Controller for a Standalone Multi-Source Power System. *Technologies* **2023**, *11*, 22. [CrossRef]
11. Fathy, A.; Kassem, A.; Zaki, Z.A. A Robust Artificial Bee Colony-Based Load Frequency Control for Hydro-Thermal Interconnected Power System. *Sustainability* **2022**, *14*, 13569. [CrossRef]
12. Farahani, M.; Ganjefar, S.; Alizadeh, M. PID controller adjustment using chaotic optimisation algorithm for multi-area load frequency control. *IET Control Theory Appl.* **2012**, *6*, 1984–1992. [CrossRef]
13. Gopi, P.; Alluraiah, N.C.; Kumar, P.H.; Bajaj, M.; Blazek, V.; Prokop, L. Improving load frequency controller tuning with rat swarm optimization and porpoising feature detection for enhanced power system stability. *Sci. Rep.* **2024**, *14*, 15209. [CrossRef] [PubMed]
14. Mohamed, M.A.E.; Jagatheesan, K.; Anand, B. Modern PID/FOPID controllers for frequency regulation of interconnected power system by considering different cost functions. *Sci. Rep.* **2023**, *13*, 14084. [CrossRef]
15. Sondhi, S.; Hote, Y.V. Fractional order PID controller for load frequency control. *Energy Convers. Manag.* **2014**, *85*, 343–353. [CrossRef]
16. Gupta, D.K.; Dei, G.; Soni, A.K.; Jha, A.V.; Appasani, B.; Bizon, N.; Srinivasulu, A.; Nsengiyumva, P. Fractional order PID controller for load frequency control in a deregulated hybrid power system using Aquila Optimization. *Results Eng.* **2024**, *23*, 102442. [CrossRef]
17. Shawqran, A.M.; Attia, M.A.; Mekhamer, S.F.; Kotb, H.; Ibrahim, M.A.; Mordi, A. Enhancing Load Frequency Control in Power Systems Using Hybrid PIDA Controllers Optimized with TLBO-TS and TLBO-EDO Techniques. *Processes* **2025**, *13*, 1532. [CrossRef]
18. Khadanga, R.K.; Kumar, A.; Panda, S. A novel modified whale optimization algorithm for load frequency controller design of a two-area power system composing of PV grid and thermal generator. *Neural Comput. Appl.* **2019**, *32*, 8205–8216. [CrossRef]
19. Rani Bhupathiraju, S.; Rao Pedakota, K. Load Frequency Control of Hybrid Power System with PIDD Controller in Presence of Electric Vehicles. *J. Electr. Syst.* **2024**, *20*, 5093–5102.
20. Shouran, M.; Anayi, F.; Packianather, M. Design of sliding mode control optimised by the Bees algorithm for LFC in the Great Britain power system. *Mater. Today Proc.* **2022**, *52*, 937–943. [CrossRef]
21. Mohanty, B. TLBO optimized sliding mode controller for multi-area multi-source nonlinear interconnected AGC system. *Int. J. Electr. Power Energy Syst.* **2015**, *73*, 872–881. [CrossRef]
22. Kumar, A.; Anwar, M.N.; Kumar, S. Sliding mode controller design for frequency regulation in an interconnected power system. *Prot. Control Mod. Power Syst.* **2021**, *6*, 6. [CrossRef]
23. Pandey, S.K.; Mohanty, S.R.; Kishor, N.; Catalão, J.P.S. An Advanced LMI-Based-LQR Design for Load Frequency Control of an Autonomous Hybrid Generation System. In *IFIP Advances in Information and Communication Technology*; Springer: Berlin/Heidelberg, Germany, 2013.
24. Garg, R.; Mittal, A.; Syed, K.; Asim, M.; Chakravorty, A.; Goyal, S. Linear Quadratic Regulator (LQR)-Based Load Frequency Control in Power Systems. In Proceedings of the 2024 2nd World Conference on Communication and Computing WCONF, Raipur, India, 12–14 July 2024. [CrossRef]
25. Amiri, F.; Hatami, A. Load frequency control for two-area hybrid microgrids using model predictive control optimized by grey wolf-pattern search algorithm. *Soft Comput.* **2023**, *27*, 18227–18243. [CrossRef]
26. Mokhtar, M.; Marei, M.I.; Sameh, M.A.; Attia, M.A. An Adaptive Load Frequency Control for Power Systems with Renewable Energy Sources. *Energies* **2022**, *15*, 573. [CrossRef]
27. Rahangdale, C.K.; Shukla, S.P.; Singh, S.K. Automatic Generation Control Using Model Reference Adaptive Control (MRAC) Scheme in a Multi Area Power System. *NeuroQuantology* **2021**, *19*, 811–820. [CrossRef]
28. Chuang, N. Robust H^{∞} load-frequency control in interconnected power systems. *IET Control Theory Appl.* **2016**, *10*, 67–75. [CrossRef]

29. Barakat, M. Optimal design of fuzzy-PID controller for automatic generation control of multi-source interconnected power system. *Neural Comput. Appl.* **2022**, *34*, 18859–18880. [CrossRef]
30. Obaid, Z.A.; Cipcigan, L.M.; Muhssin, M.T. Fuzzy hierarchal approach-based optimal frequency control in the Great Britain power system. *Electr. Power Syst. Res.* **2016**, *141*, 529–537. [CrossRef]
31. Feleke, S.; Pydi, B.; Satish, R.; Kotb, H.; Alenezi, M.; Shouran, M. Frequency Stability Enhancement Using Differential-Evolution- and Genetic-Algorithm-Optimized Intelligent Controllers in Multiple Virtual Synchronous Machine Systems. *Sustainability* **2023**, *15*, 13892. [CrossRef]
32. Shouran, M.; Anayi, F.; Packianather, M.; Habil, M. Different Fuzzy Control Configurations Tuned by the Bees Algorithm for LFC of Two-Area Power System. *Energies* **2022**, *15*, 657. [CrossRef]
33. Sahu, B.K.; Pati, S.; Mohanty, P.K.; Panda, S. Teaching-learning based optimization algorithm based fuzzy-PID controller for automatic generation control of multi-area power system. *Appl. Soft Comput.* **2015**, *27*, 240–249. [CrossRef]
34. Barakat, M. Novel chaos game optimization tuned-fractional-order PID fractional-order PI controller for load–frequency control of interconnected power systems. *Prot. Control Mod. Power Syst.* **2022**, *7*, 16. [CrossRef]
35. Ali, E.S.; Abd-Elazim, S.M. BFOA based design of PID controller for two area Load Frequency Control with nonlinearities. *Int. J. Electr. Power Energy Syst.* **2013**, *51*, 224–231. [CrossRef]
36. Sahu, R.K.; Panda, S.; Padhan, S. A hybrid firefly algorithm and pattern search technique for automatic generation control of multi area power systems. *Int. J. Electr. Power Energy Syst.* **2015**, *64*, 9–23. [CrossRef]
37. Jia, H.; Wen, Q.; Wang, Y.; Mirjalili, S. Catch fish optimization algorithm: A new human behavior algorithm for solving clustering problems. *Clust. Comput.* **2024**, *27*, 13295–13332. [CrossRef]
38. Liu, T.; Wang, R.; Han, B.; Wang, R. Advanced Multi-Objective Optimization for Laser Cladding of H13 Die Steel with CFOA. *Materials* **2025**, *18*, 1617. [CrossRef]
39. Ibrahim, A.-W.; Xu, J.; Farh, H.M.H.; Al-Shamma'a, A.A.; Yang, Y.; Shi, Z.; Zafar, M.H. An efficient linear-extrapolation catch-fish algorithm for maximizing the harvested power from thermoelectric generators sources. *Appl. Therm. Eng.* **2025**, *268*, 125916. [CrossRef]